7

Case Studies

7.1 Introduction

A number of case studies are now presented to show applications of the concepts illustrated in the previous chapters. After a succinct introduction of some aspects of data acquisition and digital control, three case studies are presented, namely a friction damper-based suspension unit for a saloon car, a magnetorheological damper-based seat suspension for vehicles not equipped with primary suspensions and a semi-active suspension system with magnetorheological dampers for heavy vehicles where the emphasis is not only on ride comfort but also on road damage reduction.

7.1.1 Some Aspects of Data Acquisition and Control

The reader is assumed to be familiar with the fundamental theoretical concepts of computer-based data acquisition and digital control (Shannon theorem, Nyquist theorem and digital-to-analogue and analogue-to-digital conversion). For furthering the topic the reader can refer to the numerous textbooks on the subject (*e.g.*, Leigh, 1992). Data acquisition and real-time control can be implemented using an embedded microprocessor architecture, a PC or a programmable logic controller (PLC) equipped with one or more I/O cards. Commercial data acquisition and control cards are made to acquire a variety of input signals and issue a variety of output signals including not only digital and analogue (*e.g.*, 0–10 V, ± 5 V, 4–20 mA) signals but also more specialised signals (*e.g.*, those produced by thermocouples, thermoresistances, solenoid valves, servovalves, vibration sensors, frequency modulated signals *etc.*). Signals are properly conditioned (filtered, amplified, modulated, demodulated *etc.*) by appropriate hardware within the card or via software.

In the case studies described an off-the-shelf card was used. The card was capable of receiving up to 16 single-ended channels with 12-bit resolution. Depending upon the transducers output and actuators input range, the card I/O

range could be configured. For instance in the applications described, analogue inputs were configured to have a unipolar range of 0–10 V and analogue outputs a bipolar range of ±5 V. This implies that the mean value of the quantisation error is 0.025 V, which is negligible with respect to the range of the converter[2] and in the suspension application does not produce any appreciable deterioration of the controller performance.

The card can be made to operate in clocked D/A mode; in this mode its clock is set up to produce the required sampling frequency. In the light of the Shannon theorem, considering the frequency content of the vehicle dynamic response, the sampling frequency can be set to 100 Hz. The total delay introduced in the sampling, holding and multiplexing phases is negligible.

For data acquisition, effective software is key. In the work described, a commercial data acquisition package and an in-house frequency response analyser software developed at the University of Bath (UK) were employed.

Digital closed-loop control must be implemented in real time, and therefore an environment with a deterministic operating system is required. This can be achieved with an embedded architecture or a PLC. Typically PLCs are used in industrial plants where a vast number of loops need to be controlled or monitored within the framework of a hierarchical (pyramidal type) distributed architecture. A PLC is often interfaced with a PC (often referred to as a HMI, a human–machine interface) for graphic display of the controlled plant parameters. I/O signals can be either hardwired or connected via a network (sometimes referred to as remote I/O). Signals, appropriately routed, can also be transferred to other PCs or PLCs over the network, using a variety of transmission media (*e.g.*, serial links, Ethernet or fibre optics) and appropriate protocols. A typical automotive protocol is the controller area network (CAN bus). Control software can be written in a graphical language (Ladder-like) or in C/C++. Fast dynamics routines can also be written in Assembly language to optimise performance.

Closed-loop control software in the applications described was written in C. Good programming practice suggests to write software in modular form, and develop a user interface that allows the entry of the key configurable parameters of the control algorithm, enabling data to be saved to file for off-line post-processing.

In automotive applications embedded architectures are used and feedback signals are either hardwired using shielded cables (and additional low-pass filtering stages are present in the on-board electronics) or transmitted over the network. Furthermore dedicated circuitries are present to increase the noise rejection.

---

2. The resolution V_0 of a converter can be calculated with the following expression that links range of the converter, resolution and number of bits:

$[K]\ Log_{10}\ 2 = Log_{10}\{(V_{max} - V_{min})/V_0 + 1\}$,

where $[K]$ is an integer that represents the number of bits and $V_{max} - V_{min}$ is the range of the converter.

7.2 Car Dynamics Experimental Analysis

A car, thought of as a rigid body unilaterally constrained by the road, is a 6DOF system having three translational (forward and backward motion, side slip and bounce) and three rotational (roll, pitch and yaw) degrees of freedom.

From the viewpoint of assessing the ride performance of a suspension system, bounce, roll and pitch motions are the most pertinent. Side slip, which occurs only for a lack of adhesion, and yaw are of interest mainly to handling studies.

At the outset it is necessary to specify the inputs which excite car dynamic responses of interest and which best represent real conditions on the road. Vehicle driving tests in controlled conditions would appear to be the most natural solution. However it is also possible to emulate the road input with a road simulator. This allows measurements to be made in more controlled conditions; besides, it permits tests which are not feasible on a road to be carried out (*e.g.*, sine wave inputs or the excitation of single suspension units separately to mimic a quarter-car-like behaviour). Moreover on a road simulator the level of external disturbances is reduced or even eliminated (*e.g.*, wind gust) compared to a road test, and hence tests are more repeatable.

Preliminary tests on the car equipped with its original viscous damper are necessary in order to have a set of data to benchmark a semi-active system. In the following developments it will be described how to practically carry out vehicle measurements and how to process data effectively.

7.2.1 The Experimental Set-up

The heart of the vehicle testing equipment is the four-poster road simulator. This is essentially composed of four hydraulic actuators on which the vehicle under testing (a Ford Orion) is placed (Figure 7.1).

The main features of the road simulator available at the University of Bath are now briefly described to identify its potential and its limits. Each hydraulic actuator is position-controlled through a servovalve. The rig is operated via a human–machine interface PC where software manages and supervises all the operations. It is possible to select elementary inputs (sine waves, half-sine waves, square waves) in the 0–25 Hz frequency range and ±125 mm amplitude range. The relative phase shift among the actuators can be controlled as well. In this way pure bounce, roll and pitch inputs, and other customised inputs, can be generated. Furthermore, it is possible to create user-defined waveforms by composing elementary functions via a graphical editor.

In order to gain an understanding of the vehicle dynamic phenomena of interest and to provide a comprehensive set of data to assess suspension performance, tests with the following inputs are essential:

- sinusoidal input to a single wheel
- bounce, roll and pitch tests with sinusoidal input
- pseudo-random input
- bump test

Sinusoidal waveforms do not represent any realistic road condition. However they are simple and well-known inputs and they allow the use of frequency-domain methods for manipulating data. Sinusoidal tests give a first clue to the effectiveness of the suspensions: they permit an assessment of how controlled suspensions behave with respect to passive suspensions.

Fig. 7.1. Test vehicle on the four-poster road simulator

It must be remarked that, because of the non-linear behaviour of the four-poster shaker, it is not possible to obtain a truly sinusoidal motion in spite of a sinusoidal driving input voltage applied to the shaker. In addition the ride dynamic response of the passive car is linear only to a first approximation (the main non-linearities being the tyre characteristics and the hysteretic viscous damper characteristics, including mountings and rubber bushes). As a consequence of the whole system being non-linear, it is not possible to define a proper frequency response (in the control sense). For this reason the most significant plot is the RMS value (or the ratio of two RMS values, for instance the ratio of chassis and wheel accelerations versus the fundamental harmonic of the excitation frequency for a fixed input amplitude). This experimental frequency response should more appropriately be called the acceleration transmissibility ratio, because it includes the effect of all the harmonic content of the signals. However for ease of terminology the term frequency response will be used hereafter.

The passive system frequency responses are ideally expected to be worse (*i.e.*, with larger values) than the semi-active frequency responses in the working frequency range.

This is a first crucial assessment in the frequency domain before further investigations in order to evaluate the properties of the responses in the time domain (harmonic content, peak values, higher-derivative trends, peak values *etc.*).

The vehicle is instrumented with four accelerometers and one displacement transducer mounted on the axle where the semi-active damper is fitted. Two accelerometers are mounted on each rear wheel, connected through small cylinders bolted on the wheels. The connections to the vehicle must be made as compact and stiff as possible in order to reduce unwanted vibration which could affect the measurement. The other two accelerometers are fixed on the chassis of the car, close to each rear suspension. Accelerometers have a principal axis of sensitivity, therefore they need to be mounted vertically in order to measure the vertical component of chassis and wheel acceleration. The calibration of these devices is based on gravity (by interpolating readings at +1 g, 0 and –1 g). Because of their sensitivity to acceleration due to gravity, it might be necessary to compensate (in hardware or in software) the offset of 1 g that they may introduce.

Signals from the transducers are manipulated in conditioning cards. As mentioned in Section 7.1.1, most conditioning circuitries are essentially composed of an amplification stage followed by a filtering stage. A stabilised power supply provides the required constant voltage to the controller. Pre-amplification is necessary to make the signal more robust, increasing its immunity to noise and making it less interference sensitive. The amplifier gain must be suitably chosen considering the order of magnitude of car vertical accelerations (a good choice could be 1g =10 V for instance). The grounding is done through an earth resistance on the metallic trolley carrying the equipment; the ground is unique to avoid earth loops.

A critical stage of the conditioning chain is filtering. Acceleration is typically a noisy signal: stray effects due to the mounting, rubber bushes, friction *etc.* are picked up by the transducer and therefore it is necessary to low-pass filter the signal. The break frequency of the filter must be chosen trading off among different conflicting requirements: if it is too low it introduces an undesired phase lag and further it smoothes the waveforms by cutting off the high-frequency harmonic content. This only slightly affects integral parameters like the RMS (higher-order harmonics typically have small amplitudes). However it can diminish the actual value of some time-domain information such as peak acceleration values or jerk content which are comfort related. These need to be quantified properly (particularly in a controlled suspension with a switching control logic). On the other hand if the break frequency is too high, a significant level of noise can be superimposed on the signal, affecting not only its readability but also the accurate evaluation of its RMS. In addition, a high level of noise could introduce chattering if acceleration signals were used in a switching logic.

The choice of an appropriate break frequency is a trial-and-error process and can be initially performed with an analogue, manually-adjustable filter. In the applications investigated a second-order Butterworth filter with a break frequency of 40 Hz appeared to be appropriate. With this choice the phase lag introduced is only 10˚ at 5 Hz. Digital filtering is another option too.

The relative displacement is measured with a position transducer mounted between body and wheel. An externally mounted LVDT is not appropriate as, when the car undergoes testing, tyre torsional modes may turn the wheels, with a risk of damaging the device. Mounting connections through plastic bolts and rose joints are not always sufficient to provide protection. A pull-wire displacement

transducer is instead a better choice. This potentiometric device is safe, since the position is measured with a flexible wire, and not a rigid rod. Potentiometers (depending on the materials they are made of, *e.g.*, hybrid conductive plastic) have an extremely high resolution, resulting in a very clean measured signal; no filtering is in fact necessary. In order to calibrate it accurately, a stepper motor can be employed. Finally measurements need to be carried out with tyres inflated at their rated pressures and with wheel brakes on to minimise tyre torsional vibration, which tends to rotate them.

7.2.2 Post-processing and Measurement Results

As far as sinusoidal tests are concerned the most meaningful data are the time responses and the ratio of chassis to wheel RMS acceleration. The ride model of the car is supposed to be linear to a first approximation; this implies that the acceleration ratio is equal to the velocity and displacement ratios:

$$\frac{a_1}{a_2} = \frac{j\omega v_1}{j\omega v_2} = \frac{\omega^2 x_1}{\omega^2 x_2}, \tag{7.1}$$

a_i , v_i , x_i being, respectively, chassis and wheel (subscripts 1 and 2) acceleration, velocity and displacement. Hence transmissibility curves can be readily obtained.

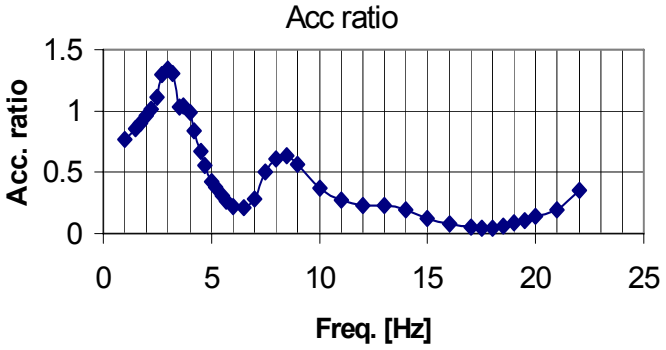

Fig. 7.2. Body-to-wheel acceleration ratio of the rear right corner of the car. Sinusoidal input to one wheel, amplitude: 3 mm

A simple test to verify the amount of linear behaviour of the passive car can be carried out by applying inputs with three different amplitudes. The closer the three responses are to one another the more the system approximates linear behaviour. Figure 7.2 shows the response of the car when only one wheel is excited; the ratio of body over wheel RMS acceleration is plotted.

The four-poster shaker actuator generates a sinusoidal waveform with a peak value of 3 mm in the range 1–22 Hz. In the car response three resonances are evident; the first one is the chassis resonance at about 3 Hz; this is fairly high:

typically this resonance occurs at about 1.5 Hz. This shift is essentially due to the small portion of sprung mass loading the suspension strut, since only the rear right corner of the car is shaken. The second resonance is at about 8.5 Hz; this is due to cross-coupling effects: around that frequency range a compound motion of bounce, roll and pitch is present; an engine mounting resonance is also possible. Eventually the wheel-hop resonance occurs at 18 Hz, although it is not readily recognisable on the graph of Figure 7.2; however if the wheel acceleration response is plotted (Figure 7.3) the resonance becomes clear.

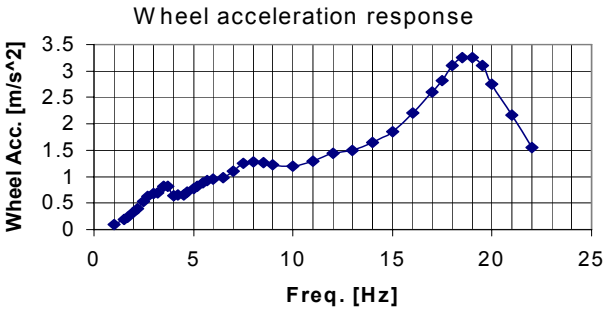

Fig. 7.3. Rear right wheel acceleration response. Sinusoidal input to one wheel, amplitude: 3 mm

Figure 7.4 shows the same response as above when three different input amplitudes (3 mm, 5 mm and 7 mm) are applied (for the purpose of testing linearity). The differences among the three graphs are reasonably small; hence it is possible to state that the non-linear effects, although present, are not so significant and the hypothesis of linearity is fairly realistic within the amplitude range of the signals. Non-linear effects occur typically with large signals (although small signals can also excite non-linear phenomena).

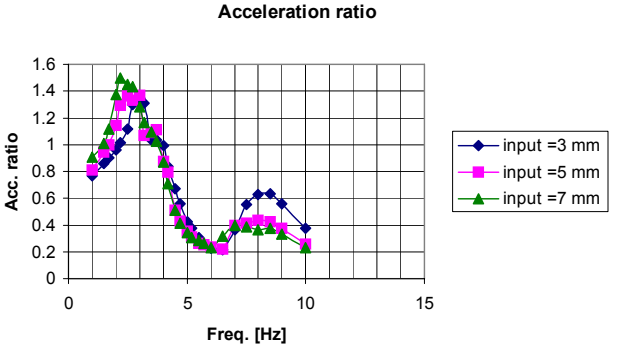

Fig. 7.4. Body-to-wheel acceleration ratio of the rear right corner of the car. Sinusoidal input to one wheel, amplitudes: 3 mm, 5 mm, 7 mm

Figures 7.5 and 7.6 depict two responses in the time domain: relative body-to-wheel displacement and body acceleration (units have been scaled), in response to a 3 mm amplitude sinusoidal signal at a frequency of 2.5 Hz. The traces are nearly sinusoidal. This further confirms the hypothesis of linearity.

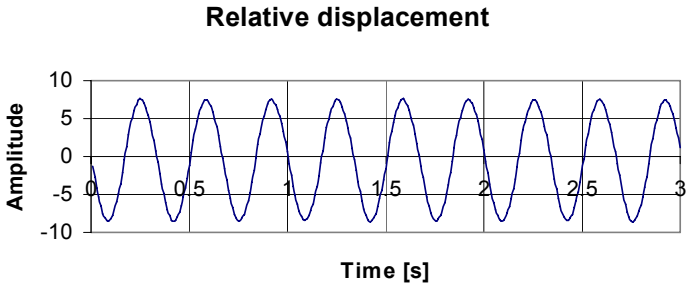

Fig. 7.5. Relative displacement time trend. Sinusoidal input to one wheel, amplitude: 3 mm, frequency: 2.5 Hz

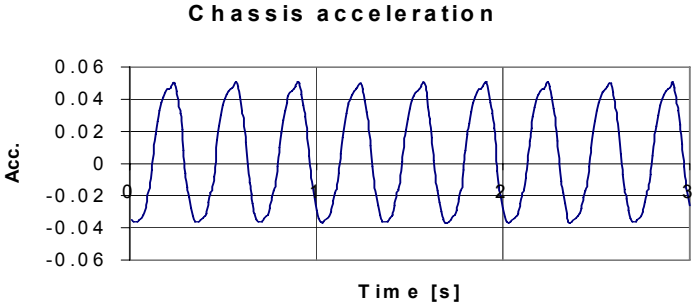

Fig. 7.6. Chassis acceleration time trend. Sinusoidal input to one wheel, amplitude: 3 mm, frequency: 2.5 Hz

For subsequent studies, the frequency range is limited to 6 Hz. Such a range is sufficient to show all the main dynamic phenomena associated with the chassis, in response to bounce, roll and pitch inputs. Figure 7.7 shows the rear right and rear left corner responses of the car to a pure bounce input, applied to all four wheels.

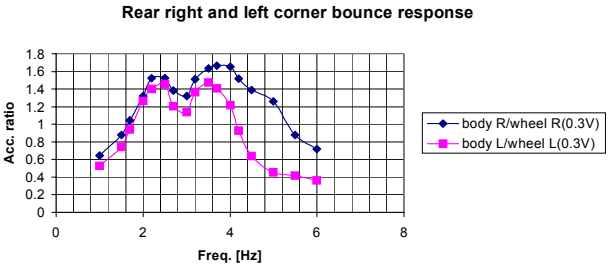

Fig. 7.7. Body-to-wheel acceleration ratio of the rear of the car. Sinusoidal bounce input to all wheels, amplitude: 3 mm

The right and left corner trends exhibit some differences; this is mainly because the centre of gravity of the car does not exactly pass through the vertical plane of symmetry. Two resonances are evident from the figure: the first (around 2.3 Hz) is the bounce resonance while the second resonance (around 3.8 Hz) is due to the pitch–bounce coupled motion. In order to identify which is the dominant parasitic motion (with respect to pure bounce) responsible for that spurious resonance, two more accelerometers can be mounted on the front of the car above each suspension and the relative phase shift recorded. A phase shift of about 180˚ is associated with roll motion, while a null phase shift corresponds to pitch motion. At the spurious resonance of 3.8 Hz the measured phase shift was about 40˚, and hence this resonance is mainly due to the induced pitch motion.

Pitch response is presented in Figure 7.8. Two resonances again are present as before: the pitch resonance at around 2.3 Hz, plus another one at around 3.8 Hz due to cross-coupling effects.

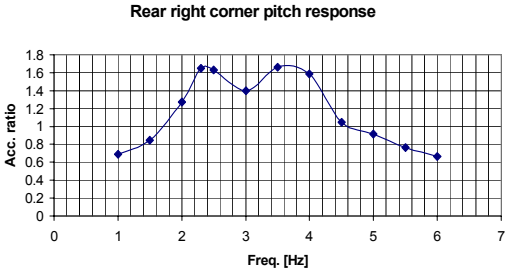

Fig. 7.8. Body-to-wheel acceleration ratio of the rear left corner of the car. Sinusoidal pitch input to all wheels, amplitude: 3 mm

Figure 7.9 shows the roll response for three different inputs applied from an external voltage signal generator (0.2 V, 0.3 V and 0.4 V corresponding to 2.74 mm, 4.11 mm, and 5.48 mm, the calibration factor being 1 V = 13.7 mm). Two resonances are clear from the graph: the roll resonance at around 2.3 Hz and another spurious cross-coupling resonance at about 6 Hz. The closeness of the three responses confirms once again the hypothesis of linearity.

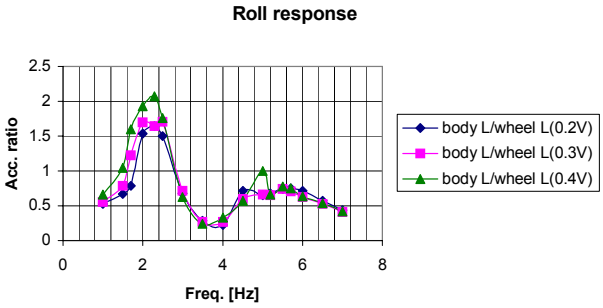

Fig. 7.9. Body-to-wheel acceleration ratio of the rear left corner of the car. Sinusoidal roll input to all wheels, amplitude: 0.2 V, 0.3 V, 0.4 V (1 V = 13.7 mm)

Figure 7.10 depicts the rear right relative displacement (body-to-wheel) response to a roll input. This is proportional to the rolling angle (relative to the wheel). The rolling angle is usually referred to the ground. However in the frequency range of interest the wheel can be considered almost steady so that the rolling angle with respect to the ground is not expected to differ very much from the one measured with respect to the wheel. As expected the resonance measured in terms of acceleration occurs at the same frequency as that of Figure 7.9.

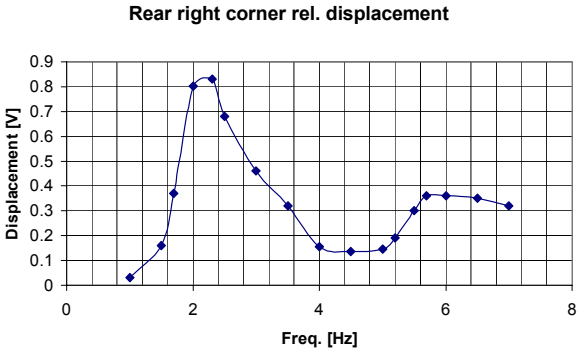

Fig. 7.10. Relative displacement of the rear-right corner of the car. Sinusoidal roll input to all wheels, amplitude: 0.2 V, 0.3 V, 0.4 V (1 V = 13.7 mm)

For the pseudo-random input test, 25-Hz filtered white noise, produced with an external noise generator, is applied to the rear-right wheel. The body acceleration time trend is plotted in Figure 7.11; its RMS value is 0.75 m/s^2.

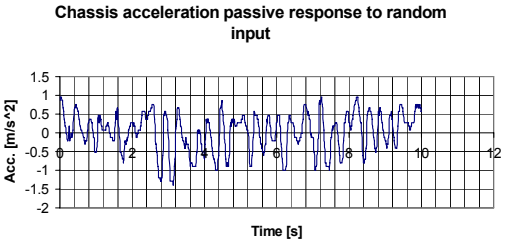

Fig. 7.11. Chassis acceleration time trend. Random input, 25-Hz filtered white noise

The last test is the bump input. A sinusoidal bump with a slight offset has been generated; the demanded input is filtered by actuator dynamics, resulting in a smoother signal. Figure 7.12 shows the response of the car to a bump applied at the rear right wheel.

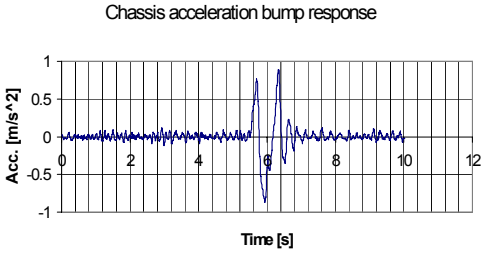

Fig. 7.12. Chassis acceleration time trend. Sinusoidal bump input, amplitude: 30 mm

The most meaningful parameters in a bump test are peak acceleration and number of oscillations. In this case the max overshoot and undershoot are symmetrical with a value of ±0.85 m/s^2 and the decay of oscillations indicate an equivalent damping ratio of approximately 0.3.

7.2.3 Suspension Spring and Tyre Tests

If accurate figures for spring and tyre stiffness are required, an experimental bench test assessment must be undertaken. This subsection describes a simple method to measure the suspension spring stiffness and the tyre stiffness.

Spring stiffness tests can be carried out by cyclically loading the spring in a material testing machine with a periodic force applied quasi-statically. The compression of the spring under the load can be measured with an extensometer or an LVDT and the force applied with a strain gauge. The spring characteristic is expected to be linear in the measured range. Experiments showed linearity up to a deflection of 200 mm. Such a deflection is far larger than the one experimented in a saloon car under normal conditions. This validates the hypothesis of linearity and allows a linear model to be used for the spring. The spring static stiffness recorded

for the vehicle under test was 19 kN/m. No hysteresis is present, the spring being a steel coil.

The same type of test can be carried out on the tyre. It is possible to define a tyre radial stiffness, which is the one of interest in ride analysis, as well as a tyre lateral stiffness, which is more of interest in handling behaviour.

The experimental set-up is roughly the same; however, in this case, it is important to specify how the load is applied (concentrated or distributed) as the stress distribution is different. A load distributed over a small area, however, better represents the forces transmitted from the road.

The typical trend is expected to be slightly non-linear with some hysteresis because rubber is a viscoelastic material. The equivalent linear value of stiffness, measured as the slope of the line interpolating the points corresponding to null force and maximum force, was 74 kN/m. The effective stiffness is twice this value because the tyre as loaded for the test can be thought of as two springs in parallel. If the tyre is loaded from the top the stiffness measured will be half that experienced by a load at the axle, which is what is needed for vehicle dynamics.

7.3 Passively Damped Car Validation

Experimental data can be used for the validation of the 7DOF mathematical model described in Chapter 2. The validation process ought to be carried out over the whole range of the expected operating conditions. However in practice a selection of relevant inputs must be made, extrapolating the model behaviour for all other possible inputs.

The accuracy achieved by the vehicle model has to be assessed both in the time and frequency domains. In the time domain, the simulated trends ought to reproduce the behaviour of the measured quantities, following as closely as possible the trends of the measured variables. In the frequency domain a good match of the frequency response is expected in the range of interest.

Figure 7.13 shows a comparison of measured and predicted rear right body acceleration time history at a frequency of 2.5 Hz. The experimental trend is almost sinusoidal; this confirms again the hypothesis that the behaviour of the car is reasonably linear for typical road profile amplitudes. Under such conditions the simulated behaviour is quite close to the experimental response. The model ought to work in a range of input amplitudes of the order of 10 mm; if the inputs are too large or too small they can excite unmodelled dynamics.

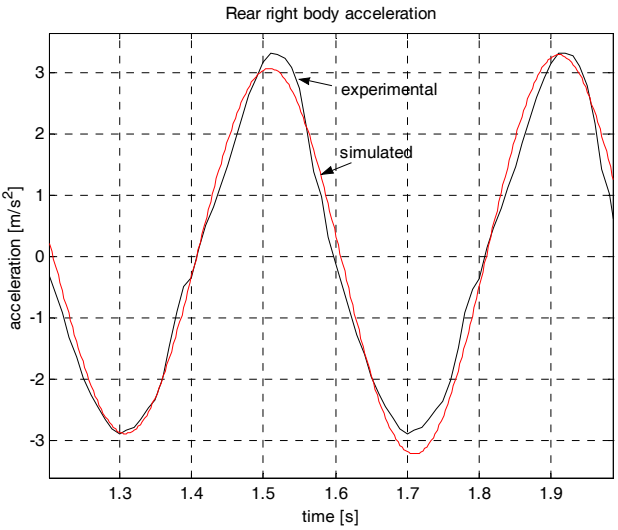

Fig. 7.13. Rear right passive acceleration; sinusoidal input to one wheel, amplitude: 7 mm; frequency: 2.5 Hz

Turning to the frequency-domain analysis, the measured RMS acceleration of the right rear body acceleration for an input excitation of 7 mm is presented in Figure 7.14 (stars on the graph). Predicted behaviour, for four different levels of viscous damping, is also shown. Up to 4 Hz the match is fairly good. At higher frequencies, the simulation overestimates the acceleration. This is presumably due to unmodelled non-linearities, principally associated with the viscous damper characteristic (the viscous damper characteristic employed in the model is obtained by linearising its actual characteristic around the origin, while the real characteristic is non-linear with different trends for bound and rebound strokes). At higher frequencies the local slope of the actual viscous characteristic is smaller than that modelled, resulting in lower damping in practice. Furthermore in a real viscous damper some hysteresis is present, attributable partly to the rubber bushes and parasitic friction as well as to the dissipative internal forces within the hydraulic oil. This explains the mismatch between the experimental data and simulation at frequencies higher than the chassis resonance frequency.

At 8.5 Hz a further resonance is present, due to either the engine mounting or to the induced yaw; such a resonance is not predicted by the model, which would need further degrees of freedom to include these dynamic phenomena. The tyre model is not sophisticated since ride is the main issue here. However highly complicated tyre models are essential in handling studies (as well as in brake/traction analysis) where lateral forces play a major role and not in ride studies where the dynamics of interest are vertical. A small amount of hysteresis is present in the tyre characteristics, but this mainly affects the behaviour around the wheel-hop resonance. The results of a sensitivity analysis, by changing the viscous coefficient in the range 350–425 Ns/m, are also depicted in the figure. Best

agreement between predicted and measured behaviour is obtained with a viscous damping coefficient of 400 Ns/m.

Therefore, the 7DOF car model captures the main features of the response both in the time and the frequency domain, up to the chassis resonance frequency. For more accurate modelling of the higher-frequency range a more complicated model would be required.

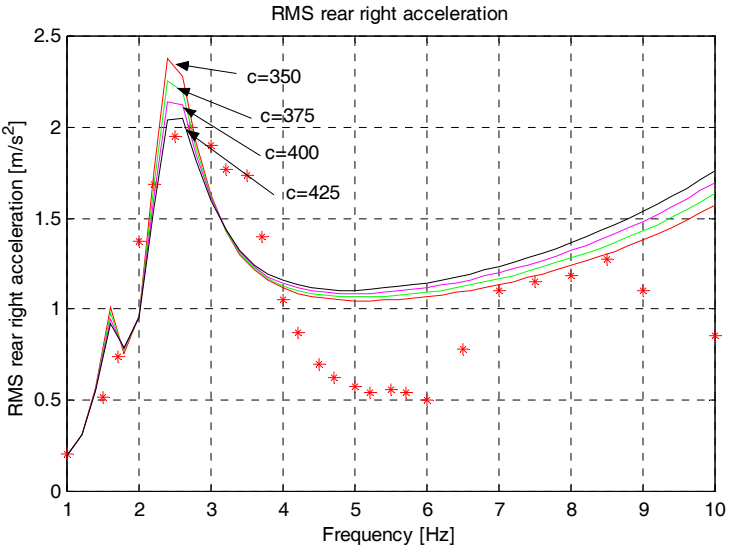

Fig. 7.14. Rear-right passive acceleration frequency response; sinusoidal input to one wheel, amplitude: 7 mm; *c* is the viscous damping coefficient in Ns/m [copyright Elsevier (2003), reproduced from Guglielmino E, Edge KA, Controlled friction damper for vehicle applications, Control Engineering Practice, Vol. 12, N 4, pp 431–443, used by permission]

7.4 Case Study 1: SA Suspension Unit with FD

This section reports the performance of a semi-active suspension unit equipped with a friction damper. After the experimental work on the damper and on its hydraulic drive described in Chapter 5, the friction damper has been installed on a vehicle under test (Figure 7.15).

Fig. 7.15. Friction damper installed on the experimental vehicle

The system supply pressure defined by the relief valve is set to 60 bar for the reasons outlined in Chapter 5. The control valve is connected to the FD, using a hose as short as possible to reduce the volume. The instrumentation is the same employed in the tests on the passively damped car. The results are presented in the following subsections. Firstly the frequency-domain performance of the semi-active FD is discussed. In this domain it is possible to make an initial comparative assessment with the benchmark viscous damper response in terms of RMS values. Subsequently an analysis in the time domain is carried out. Particular care has been given to the issue of ride comfort assessment. This issue is critical in a suspension whose control is based on a switching logic, as time trends can potentially be non-smooth and spiky, causing an uncomfortable ride.

7.4.1 Frequency-domain Analysis

The analysis in the frequency domain is based on RMS values. A comparative analysis of acceleration and working space transmissibility curves in the semi-active and passive case is presented. Figure 7.16 shows the experimentally determined acceleration transmissibility ratio for an input amplitude of 7 mm in the range 1–5 Hz compared with the original (passive) system. The controlled system out-performs the passive system over most of frequency range considered although the passive system response is marginally better up to 1.8 Hz. The controlled response exhibits three peaks: the first, at 1.7 Hz, is the semi-active system chassis resonance; this frequency is lower than the corresponding passive resonance and the peak amplitude is smaller. The inferior behaviour of the semi-active system at low frequency is due to the hydraulic circuit back-pressure, which causes a residual

constant-amplitude friction force. The small amplitudes at the lowest frequencies do not produce very significant pressure variations: in this range the constant-amplitude friction force is not negligible. When the frequency increases, the feedback signal is larger and the FD works properly. Hence, the residual friction force deteriorates the performance of the damper if the disturbance is not large, *i.e.*, on smooth roads and at low speed. This confirms that the compensation of the residual friction force via a pre-loaded spring inside the damper would be an effective remedy. Two more peaks are evident in the semi-active curve. This is a non-linear effect of the semi-active system, but in fact the resonances do not create any problem, because they are far lower in size than the corresponding passive values.

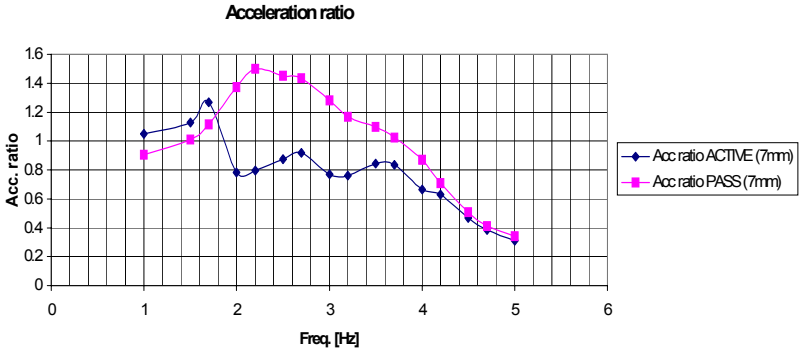

Fig. 7.16. Acceleration ratio transmissibility for passive and semi-active systems. Sinusoidal input to one wheel, amplitude: 7 mm [copyright Elsevier (2003), reproduced with minor modifications from Guglielmino E, Edge KA, Controlled friction damper for vehicle applications, Control Engineering Practice, Vol. 12, N 4, pp 431–443, used by permission]

Figure 7.17 portrays the rear-right suspension working space responses (scaled units) in both cases. Over the frequency range considered the wheel motion can be assumed to be almost steady, hence working space is a good approximation to absolute chassis displacement. The results presented show that the semi-active response is much the same as the passive response, except at the resonant frequency. This is because of the force tracking performed by the controller which inherently promotes higher displacements.

Fig. 7.17. Working space for passive and semi-active systems. Sinusoidal input to one wheel, amplitude: 7 mm [copyright Elsevier (2003), reproduced with minor modifications from Guglielmino E, Edge KA, Controlled friction damper for vehicle applications, Control Engineering Practice, Vol. 12, N 4, pp 431–443, used by permission]

Figure 7.18 depicts the acceleration response for three different input amplitudes. Within reasonable approximations they are fairly similar. This means that nonlinear effects are not very strong. Actually balance logic governing differential equation is piecewise linear and for this particular class of equations the frequency response does not depend on the input amplitude as is the case in nonlinear systems[3].

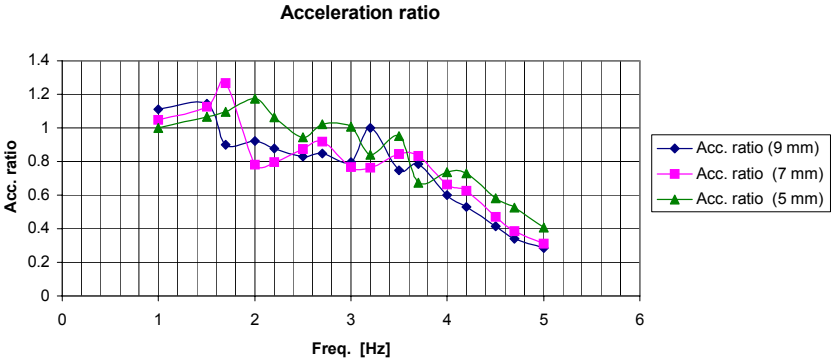

Fig. 7.18. Acceleration ratio transmissibility for semi-active system. Sinusoidal input to one wheel; amplitudes, 5 mm, 7 mm, 9 mm

3. In a linear system the RMS and peak transmissibility ratios (*e.g.*, body over wheel acceleration) are equal and independent of the input signal amplitude. In a piecewise-linear system RMS and peak transmissibility ratios are not equal but still input amplitude independent. In a nonlinear system RMS and peak transmissibility ratios are not equal and both input amplitude dependent.

Figures 7.19 and 7.20 show the effect of a change in the control law and in the friction properties. Figure 7.19 examines the effect of changing the closed-loop coefficient b from 2 to 3.33; b is the reciprocal of the friction coefficient μ, and hence its increase from 2 to 3.33 can be treated as equivalent to a decrease of the friction coefficient from 0.5 to 0.3. The performance with the reduced friction shows some deterioration over part of the frequency range: this is to be expected since, with a lower assumed friction coefficient, the force cancellation is smaller, resulting in higher accelerations.

It is of interest to evaluate how a change in the frictional characteristic would affect the performance of the control. The test of Figure 7.20 is carried out in a situation of lubricated friction. The response in dry friction regime is here compared to that in lubricated friction regime. This test is important, because lubricated friction is a realistic alternative to pure dry friction: it helps reduce stiction and is potentially advantageous in terms of heat dissipation between the friction surfaces.

At low frequencies the dry friction system response is better than the lubricated friction system response although both are worse than the passive response. In the central frequency band the lubricated friction response is better, but at higher frequencies the opposite holds.

Overall, the performance of the controlled suspension is superior to the passive case and is not worsened by lubrication.

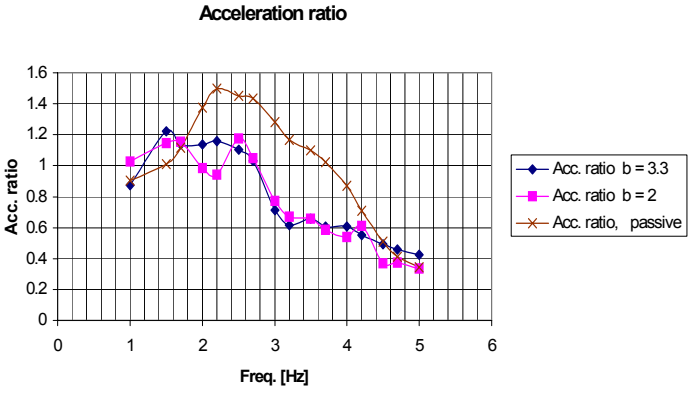

Fig. 7.19. Acceleration transmissibility ratio for passive and semi-active systems varying controller gain; sinusoidal input to one wheel, amplitude: 7 mm [copyright Elsevier (2003), reproduced with minor modifications from Guglielmino E, Edge KA, Controlled friction damper for vehicle applications, Control Engineering Practice, Vol. 12, N 4, pp 431–443, used by permission]

From the foregoing investigations involving changes in the feedback coefficient b (equivalent to a change in dry friction coefficient) and the nature of the lubrication regime, the robustness of the scheme, in a practical sense, has been experimentally verified. Moreover, the semi-active system remains generally superior to the passive system, even in the presence of these changes.

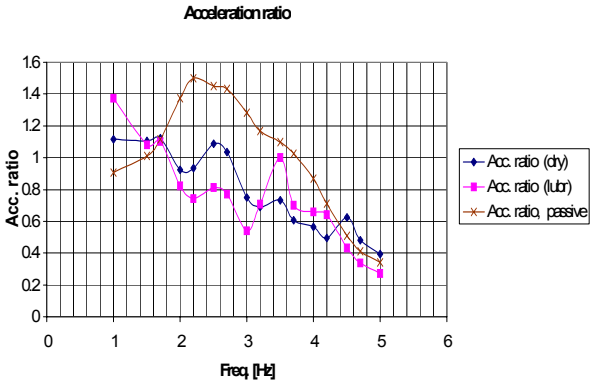

Fig. 7.20. Acceleration ratio transmissibility for passive and semi-active systems; sinusoidal input to one wheel, amplitude: 7 mm [copyright Elsevier (2003), reproduced with minor modifications from Guglielmino E, Edge KA, Controlled friction damper for vehicle applications, Control Engineering Practice, Vol. 12, N 4, pp 431–443, used by permission]

Figure 7.21 shows the effect on RMS chassis acceleration of changing the control law.

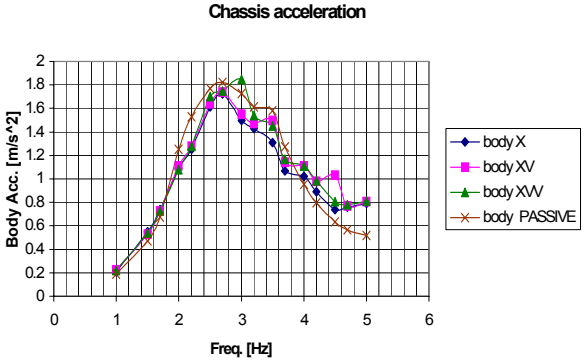

Fig. 7.21. Chassis acceleration transmissibility for passive and semi-active systems; sinusoidal input to one wheel, amplitude 7 mm

The performance of three types of controllers are compared. These are:

- a pure position feedback ($b = 2.5$, $z_1 = 0$, $z_2 = 0$) controller (X in the legend)
- a controller with position feedback in two quadrants and velocity feedback in the other two ($b = 2.5$, $z_1 = 0$, $z_2 = 0.1$; XV in the legend)
- a controller with position plus velocity feedback in two quadrants and velocity feedback in the other two ($b = 2.5$, $z_1 = 0.1$, $z_2 = 0.1$; XVV in the legend)

The pure position feedback control logic achieves the best results in terms of chassis acceleration reduction because it aims for pure spring force cancellation.

The other controller (b = 2.5, z_1 = 0, z_2 = 0.1) introduces a small viscous effect, and thus produces a slightly higher chassis acceleration. It is almost comparable with the previous controller in terms of wheel acceleration: over a part of the frequency range it is worse, but in other parts slightly better.

The final controller (b = 2.5, z_1 = 0.1, z_2 = 0.1) produces the least chassis acceleration reduction among the three types of controllers investigated and also the worst wheel acceleration. Therefore the additional viscous damping in the first and third quadrants is not advantageous.

7.4.2 Time-domain Analysis

Time domain analysis typically permits an assessment of the transient behaviour. In this context it is mainly used to assess ride quality. Figures 7.22 and 7.23 show jerk trends in the passive and semi-active cases. The latter trend presents slightly higher peak values. Jerk is obtained by numerical differentiation of the measured acceleration signal.

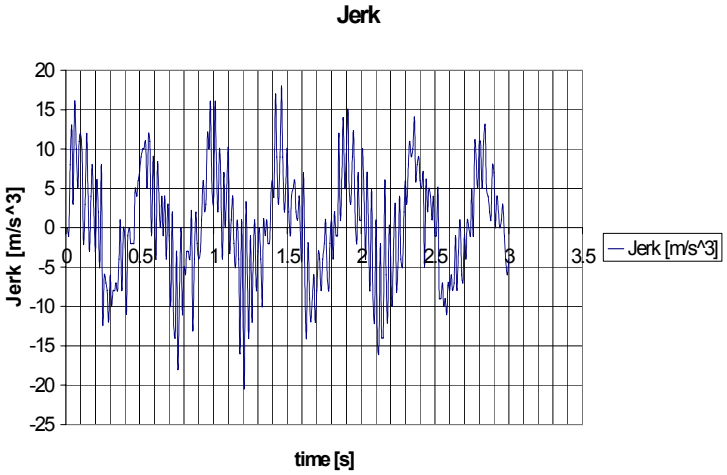

Fig. 7.22. Experimental jerk time trace for the passive system; sinusoidal input, amplitude: 3 mm, frequency: 2.2 Hz

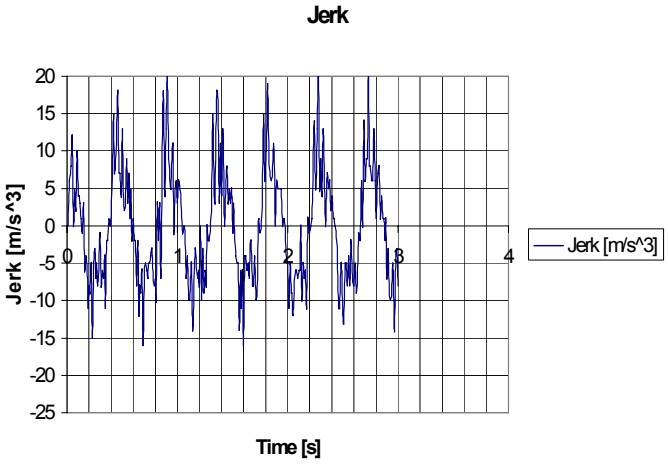

Fig. 7.23. Experimental jerk time trace for the controlled system; sinusoidal input, amplitude: 3 mm, frequency: 2.2 Hz

Next a Fourier analysis of the acceleration waveforms is presented. Although the spectrum is more appropriate to assess the degree of non-linearity rather than comfort, it is possible to establish a qualitative correlation between a high harmonic content and discomfort.

Figures 7.24–7.27 depict experimental time traces and spectra for the passive and semi-active suspension. Figures 7.24 and 7.25 show measured acceleration time histories and spectra for the passive case at frequencies of 2.2 and 4.5 Hz. At 2.2 Hz (Figures 7.24) the behaviour is fairly linear (only a negligible third harmonic is present in the spectrum).

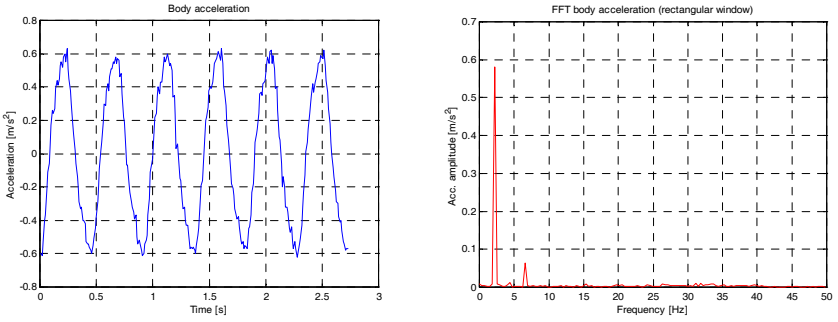

a b

Fig. 7.24. (a) Experimental acceleration time trace for the passive system; (b) experimental acceleration FFT for the passive system; sinusoidal input, amplitude: 3 mm, frequency: 2.2 Hz

The same is true at 4.5 Hz (Figure 7.26). This further validates the hypothesis of linearity of the passive system: the Fourier transform of the passive system acceleration has a small harmonic content (and to a greater extent the displacement, since acceleration is the noisiest signal).

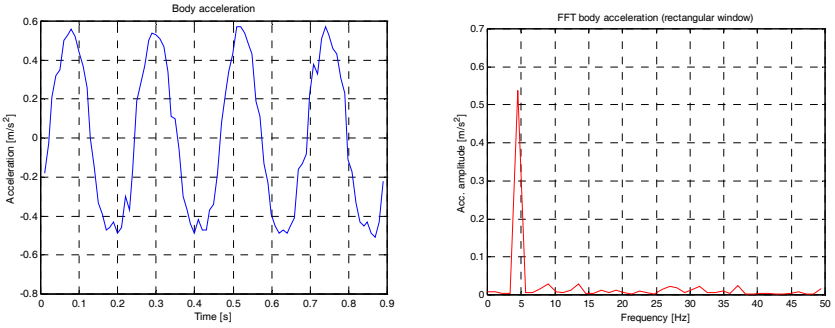

a b

Fig. 7.25. (a) Experimental acceleration time trace for the passive system; (b) experimental acceleration FFT for the passive system; sinusoidal input, amplitude: 3 mm, frequency: 4.5 Hz

Figures 7.26 and 7.27 depict the same graphs for the controlled system. The harmonic content is not very large at 2.2 Hz, but is certainly larger at 4.5 Hz and actually the acceleration time trend is fairly spiky. This spectral analysis of the acceleration has hence confirmed the qualitative correlation between jerk time trends and richer higher-harmonic content.

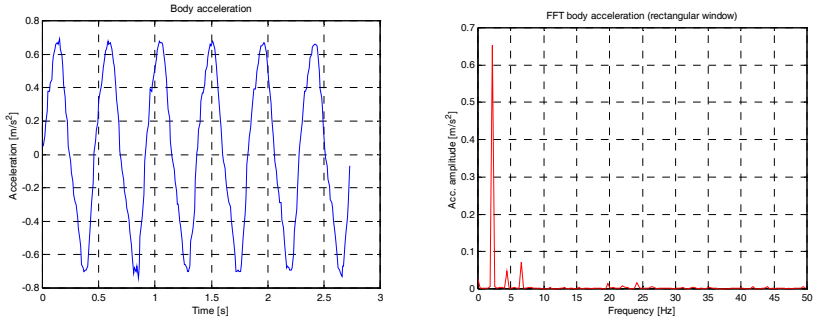

a b

Fig. 7.26. (a) Experimental acceleration time trace for the controlled system; (b) experimental acceleration FFT for the controlled system; sinusoidal input, amplitude: 3 mm, frequency: 2.2 Hz

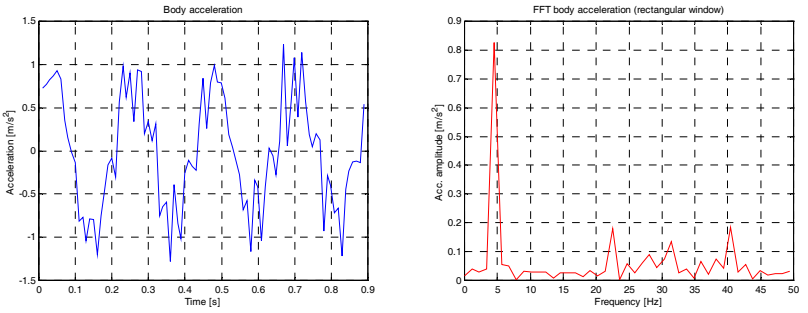

a b

Fig. 7.27. (a) Experimental acceleration time trace for the controlled system; (b) experimental acceleration FFT for the controlled system; sinusoidal input, amplitude: 3 mm, frequency: 4.5 Hz

Figure 7.28 shows the semi-active response to a pseudo-random input. The RMS of the acceleration is 0.58 m/s^2, which is smaller than in the passive case (0.75 m/s^2). Figure 7.29 shows the semi-active system response to a sinusoidal bump. The bump input is the same as in the passive case. The acceleration overshoot and undershoot for the controlled system (in the case b = 2.5, z_1 = 0, z_2 = 0) are 1.1 m/s^2 and –0.8 m/s^2 respectively, whereas for the passive system the values are ±0.85 m/s^2. The number of oscillations is the same for both cases. Thus the controlled system is slightly worse in response to a bump. This is because of the relatively slow response of the pressure control circuit. A bump can be thought as a high-frequency half-wave input (the higher the vehicle velocity, the higher the frequency) and above a certain frequency the servo-system response is not swift enough.

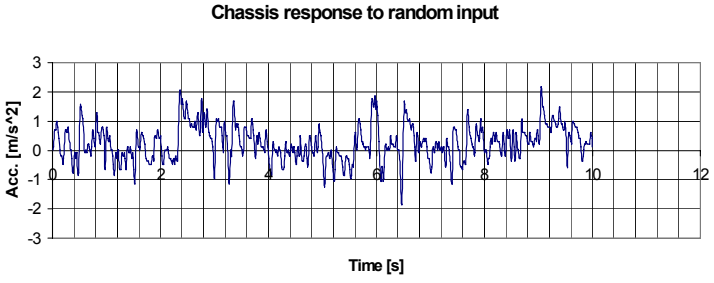

Fig. 7.28. Semi-active chassis acceleration time trend; random input: 25-Hz filtered white noise [copyright Elsevier (2003), reproduced with minor modifications from Guglielmino E, Edge KA, Controlled friction damper for vehicle applications, Control Engineering Practice, Vol. 12, N 4, pp 431–443, used by permission]

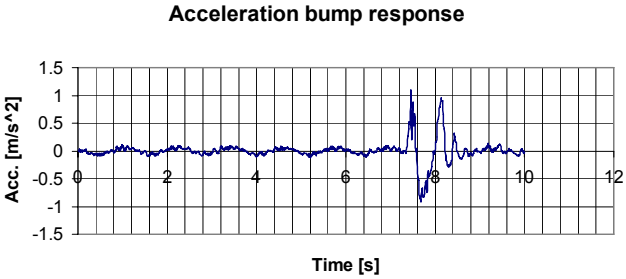

Fig. 7.29. Bump response acceleration time trace for the controlled system [copyright Elsevier (2003), reproduced with minor modifications from Guglielmino E, Edge KA, Controlled friction damper for vehicle applications, Control Engineering Practice, Vol. 12, N 4, pp 431–443, used by permission]

7.4.3 Semi-active System Validation

Having validated separately the electrohydraulic drive and the passive vehicle, the final step is the validation of the whole system. Figure 7.30 shows the predicted and measured sinusoidal time responses after the start-up transient has decayed. The simulation follows the overall trend of the measured acceleration well. The spikes in the experimental results are not captured by the model, but most of them arise from noise present in the measurements. The overall agreement can be considered acceptable.

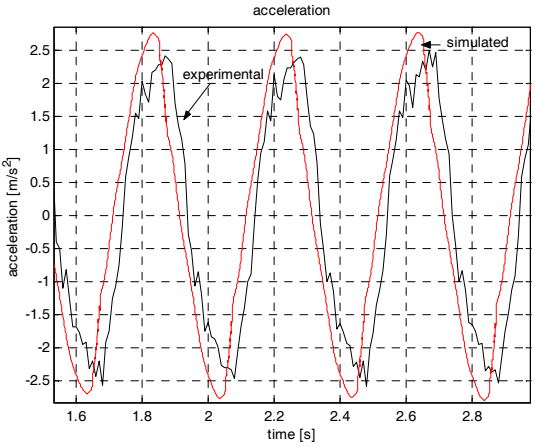

Fig. 7.30. Rear right semi-active acceleration; sinusoidal input to one wheel, amplitude: 7 mm, frequency: 2.5 Hz [copyright Elsevier (2003), reproduced with minor modifications from Guglielmino E, Edge KA, Controlled friction damper for vehicle applications, Control Engineering Practice, Vol. 12, N 4, pp 431–443, used by permission]

Considering now the frequency domain, a sensitivity analysis needs to be carried out to identify the most suitable values for the critical parameters. Figure 7.31 represents the frequency response for different friction coefficients μ between 0.1 and 0.2. At low frequency the trend is virtually independent of the friction coefficient but after the resonance the dependency gets stronger. A smaller friction coefficient produces a larger resonance peak but at higher frequency it tracks the experimental response better, and vice versa for a larger coefficient. The mismatch occurring for frequencies higher than 3.8 Hz is due to the limitations in the car model and the over-simplified model for the other three (passive) dampers, rather than to the hydraulic model of the friction damper drive. The actual value of the nominal friction coefficient of the material was 0.4. The mismatch between simulation and experiments is related to the $\frac{\mu}{\mu_{\text{assumed}}}$ ratio (see Section 5.5).

Figure 7.32 portrays the frequency response for different levels of delay between velocity and friction force created by the frictional memory effect. A change of ±50% does not produce any significant change except at the lowest frequencies.

In Figure 7.33 the effect of a change in the actuator and connecting pipe volume is considered. An increase of an order of magnitude in the volume produces a noticeable effect for frequencies above 2.5 Hz. The impact of the corresponding reduction of the valve-actuator bandwidth, following an increase in volume, is a higher acceleration. This physically occurs because the valve-actuator system cannot catch up with the higher-frequency input; therefore the effect of the residual constant friction force plays the dominant role.

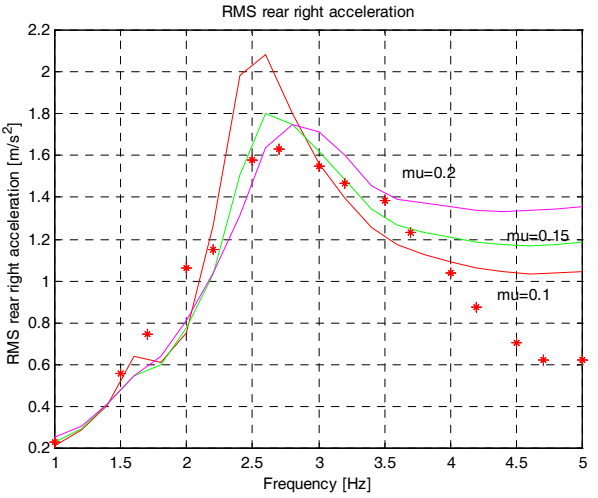

Fig. 7.31. Rear right semi-active acceleration frequency response varying friction coefficient; sinusoidal input to one wheel, amplitude: 7 mm [copyright Elsevier (2003), reproduced with minor modifications from Guglielmino E, Edge KA, Controlled friction damper for vehicle applications, Control Engineering Practice, Vol. 12, N 4, pp 431–443, used by permission]

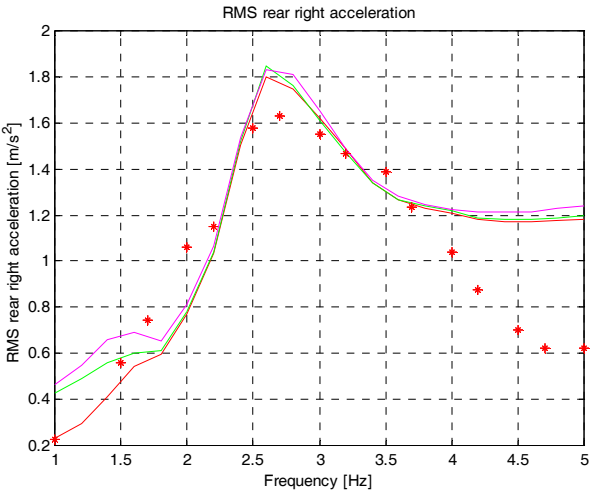

Fig. 7.32. Rear right semi-active acceleration frequency response varying frictional memory; sinusoidal input to one wheel, amplitude: 7 mm [copyright Elsevier (2003), reproduced with minor modifications from Guglielmino E, Edge KA, Controlled friction damper for vehicle applications, Control Engineering Practice, Vol. 12, N 4, pp 431–443, used by permission]

Therefore it can be concluded that simulation provides accurate results in the time domain and in the frequency domain up to almost 4 Hz. Beyond that frequency the predicted acceleration is too great.

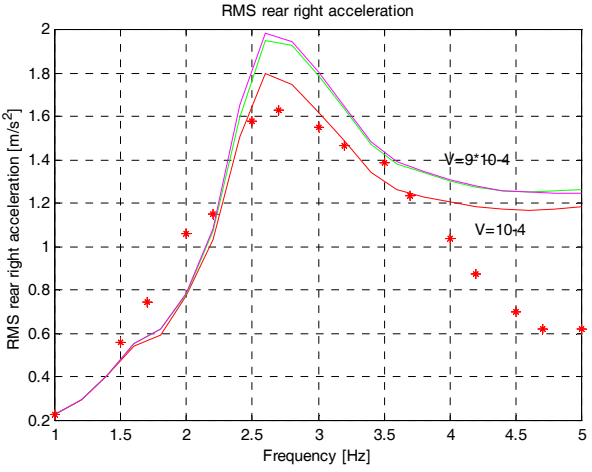

Fig. 7.33. Rear right semi-active acceleration frequency response varying volume; sinusoidal input to one wheel, amplitude: 7 mm [copyright Elsevier (2003), reproduced with minor modifications from Guglielmino E, Edge KA, Controlled friction damper for vehicle applications, Control Engineering Practice, Vol. 12, N 4, pp 431–443, used by permission]

7.5 Case Study 2: MR-based SA Seat Suspension

This case study concerns an investigation of the use of a controlled MR damper for a semi-active seat suspension in vehicles not equipped with primary suspensions (*e.g.*, some types of agricultural, forestry and roadwork vehicles). The control strategy is targeted to improve driver comfort based on a hybrid variable structure fuzzy logic controller. Variable structure control is inherently a switching logic, hence more prone to cause chattering. Fuzzy logic helps reduce chatter without penalising damper dynamic response.

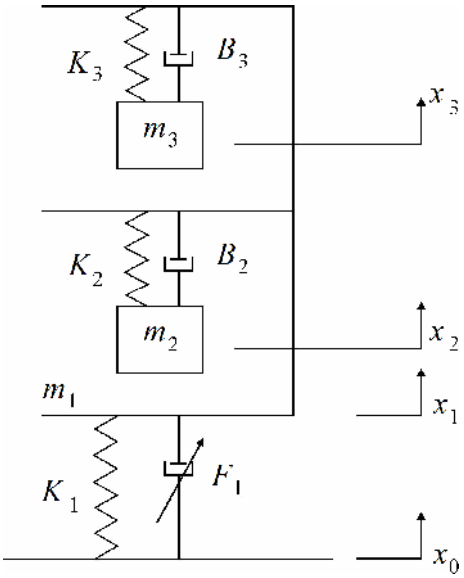

Fig. 7.34. Suspension, seat and driver model [copyright Inderscience (2005), reproduced from Guglielmino E, Stammers CW, Stancioiu D, Sireteanu T and Ghigliazza R, Hybrid variable structure-fuzzy control of a magnetorheological damper for a seat suspension, International Journal of Vehicle Autonomous Systems, Vol. 3, N 1, used by permission]

The whole system, depicted in Figure 7.34, is composed of the suspension, the seat and the driver (*i.e.*, seated body model) and can be modelled as a 3DOF system. The seat is mounted on the semi-active suspension constituted by a linear spring and the MR damper. The seat and driver model (Wei and Griffin, 1998a) consists of a rigid frame m_1 to which two masses, m_2 and m_3 are suspended. The two masses cannot be associated with particular organs of human body (refer to Chapter 3 for further details). For convenience they will be denoted as *upper* mass and *lower* mass. A driver seat suspension usually includes a linkage mechanism between the suspension unit and the seat. Its presence can be taken into account in the model by employing an equivalent value for the suspension stiffness and by appropriate scaling factors for the damping force which take into account the geometry of the linkage. Setting $x = x_1 - x_0$, the equations of motion can be written as

$$
\begin{aligned}
m_3\ddot{x}_3 &= B_3(\dot{x}_1 - \dot{x}_3) + K_3(x_1 - x_3) = f_3 \,, \\
m_2\ddot{x}_2 &= B_2(\dot{x}_1 - \dot{x}_2) + K_2(x_1 - x_2) = f_2 \,, \\
m_1\ddot{x}_1 &= F_1(x,\dot{x},z,u) + K_1 x - f_3 - f_2 \,,
\end{aligned}
\tag{7.2}
$$

where $F_1(x,\dot{x},z,u)$ is the seat suspension damping force (a Bouc–Wen model has been employed), K_1 the suspension stiffness, K_2 and K_3 the lower and upper body stiffness and B_2 and B_3 the lower and upper body damping. The value of the suspension stiffness is chosen so its natural frequency is around 1.5 Hz. Such a value corresponds to a good passive design, because it filters out the frequencies in the range 3–6 Hz, which are the worst for human comfort. The reason for this choice is to show that the controlled system can produce an improvement of the response also in presence of a good passive seat suspension. The simulation parameters are listed in Table 7.1.

Table 7.1. Key parameters employed in simulation [copyright Inderscience (2005), reproduced with minor modifications from Guglielmino E, Stammers CW, Stancioiu D, Sireteanu T and Ghigliazza R, Hybrid variable structure-fuzzy control of a magnetorheological damper for a seat suspension, International Journal of Vehicle Autonomous Systems, Vol. 3, N 1, used by permission]

Passive linear damper	B_1 = 180 Ns/m
Body upper damping	B_2 = 761 Ns/m
Body lower damping	B_3 = 458 Ns/m
Suspension stiffness	K_1 = 4500 N/m
Body upper stiffness	K_2 = 35776 N/m
Body lower stiffness	K_3 = 38374 N/m
Seat mass	m_1 = 6 kg
Body upper mass	m_2 = 33.4 kg
Body lower mass	m_3 = 10.7 kg
Bouc–Wen model coefficients	A = 2000; $\beta = \gamma$ = 2000 m^{-2}
Bouc–Wen exponent and offset force	n = 2; f_0 = 15 N

With reference to Figure 7.34, the variable the value of which must be minimised is the arithmetic mean of the RMS of lower and upper mass accelerations, $\ddot{x}_2$ and $\ddot{x}_3$, as this quantity is related to driver vertical acceleration. The frequency range of interest for comfort is up to around 6 Hz (far within the MRD bandwidth).

The aim of the control is to reduce the forces transmitted to the seat by generation of a spring-like (position-dependent damping) control force of sign opposite to that of the spring force.

The logic is implemented by controlling the solenoid current; the control logic can be expressed by the following functional equation:

$$F_1(x,\dot{x},z,u) = F(x,\dot{x},z,u(x,\dot{x}))\,, \tag{7.3}$$

where the current $u(x,\dot{x})$ is expressed by:

$$u(x,\dot{x}) = \begin{cases} a|x| & \text{if } x\dot{x} \le 0 \\ 0 & \text{if } x\dot{x} > 0\,, \end{cases} \tag{7.4}$$

a being a gain proportional to suspension spring stiffness. This balance controller is switching type and this may cause chattering problems when the controller switches from one structure to the other.

MRD dynamic response is extremely swift since it is mainly dependent upon electromagnetic dynamics and the time necessary for the oil to reach rheological equilibrium. The fast switching produces periodical acceleration and jerk peaks which degrade ride quality. Chattering problems in fast-dynamics dampers controlled via switched-type algorithms have been reported in work by Choi *et al.* (2000), who pointed out the problem in a study on sliding-mode control of electrorheological dampers. The problem can be tackled at the control level by smoothing the control action by using fuzzy logic. In this way it is possible to soften the fast switching action of the *crisp* balance controller, without the need for low-pass filters which would reduce system bandwidth, which is one the major benefits of using an MRD.

The fuzzy-controlled damping force is expressed as:

$$F_1(x,\dot{x},z,u) = F(x,\dot{x},z,\eta|x|u(x,\dot{x}))\,, \tag{7.5}$$

where $u(x,\dot{x})$ is the fuzzy controller current input and η is a gain.

The variable structure algorithm has been fuzzified by choosing as fuzzy variables the relative displacement and velocity; the linguistic variables are: negative (neg) and positive (pos). The membership functions are depicted in Figure 7.35.

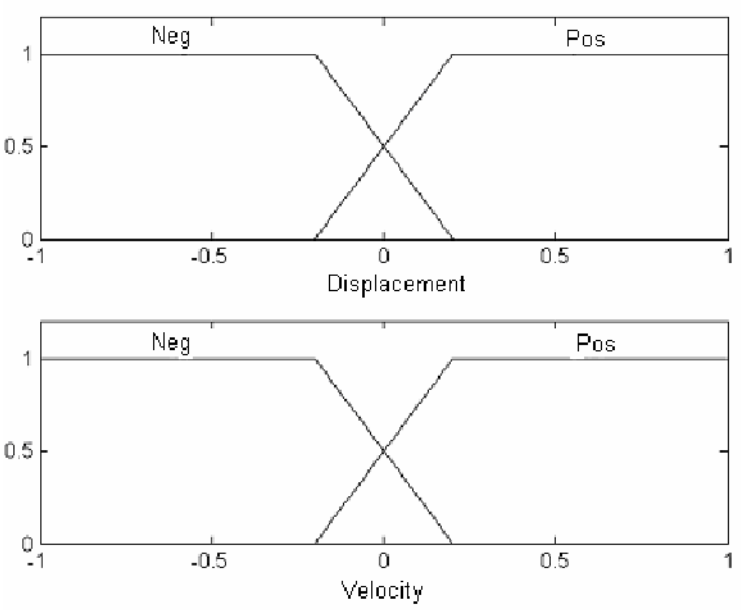

Fig. 7.35. Fuzzy logic membership functions [copyright Inderscience (2005), reproduced from Guglielmino E, Stammers CW, Stancioiu D, Sireteanu T and Ghigliazza R, Hybrid variable structure-fuzzy control of a magnetorheological damper for a seat suspension, International Journal of Vehicle Autonomous Systems, Vol. 3, N 1, used by permission]

The fuzzy controller function is a two-value function $u(x(t),\dot{x}(t)) \in [0, u_{\max}]$ where *Small* = 0 and *Big* = $u_{\max}$. The fuzzy set rules (Table 7.2) are obtained by fuzzifying the control logic defined in Equation 7.4. In this way, the transitions between the two structures are not abrupt.

Table 7.2. Fuzzy logic rules [copyright Inderscience (2005), reproduced with minor modifications from Guglielmino E, Stammers CW, Stancioiu D, Sireteanu T and Ghigliazza R, Hybrid variable structure-fuzzy control of a magnetorheological damper for a seat suspension, International Journal of Vehicle Autonomous Systems, Vol. 3, N 1, used by permission]

Velocity / **Displacement**	**Negative**	**Positive**
Negative	Small	Big
Positive	Big	Small

7.5.1 Numerical Results

The system is tested with a random input $x_0(t)$ obtained from a measured power spectral density of the seat base acceleration in operating conditions. The excitation

RMS value is σ_{x_0} = 0.02 m. Table 7.3 reports the power spectral density RMS of the controlled variables for the different controllers.

Table 7.3. Performance assessment of passive and semi-active systems [copyright Inderscience (2005), reproduced with minor modifications from Guglielmino E, Stammers CW, Stancioiu D, Sireteanu T and Ghigliazza R, Hybrid variable structure-fuzzy control of a magnetorheological damper for a seat suspension, International Journal of Vehicle Autonomous Systems, Vol. 3, N 1, used by permission]

	$\sigma_{\ddot{x}_2}$ [m/s^2]	$\sigma_{\ddot{x}_3}$ [m/s^2]	$\frac{\sigma_{\ddot{x}_2} + \sigma_{\ddot{x}_3}}{2}$ [m/s^2]
Passive linear viscous damper	3.06	3.23	3.14
Passive MRD	3.68	3.94	3.81
VSC (crisp) with MRD	2.03	2.52	2.27
Fuzzy control with MRD	2.20	2.75	2.48

A reduction of the RMS of the controlled variable of about 21% is achieved with fuzzy control, with respect to a passive system with a traditional viscous damper. The crisp controller performs slightly better (27% reduction). However the merits of the fuzzy controller are in terms of chattering reduction as is evident from Figure 7.36 where the demands for the VSC and fuzzy algorithms are presented.

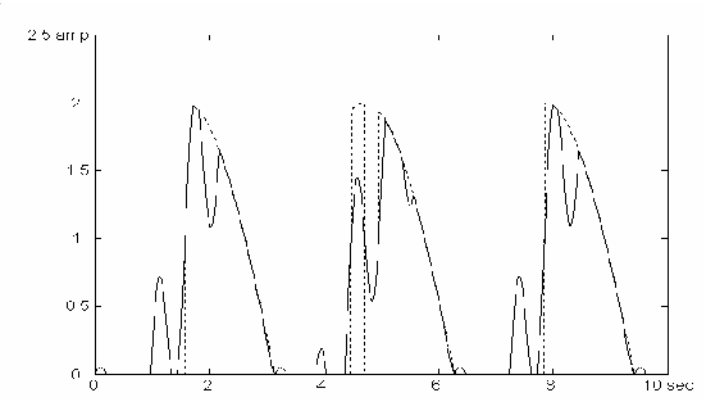

Fig. 7.36. Current demand for VSC (- - - - -) and fuzzy (——) controllers [copyright Inderscience (2005), reproduced from Guglielmino E, Stammers CW, Stancioiu D, Sireteanu T and Ghigliazza R, Hybrid variable structure-fuzzy control of a magnetorheological damper for a seat suspension, International Journal of Vehicle Autonomous Systems, Vol. 3, N 1, used by permission]

The fast switching action of the crisp controller is softened by the fuzzy algorithm and the current transitions between the on and the off state are smoother; this in

turn reduces peaks of acceleration arising in the instants of transition, thus causing improvement in the ride quality, although the RMS is slightly higher.

It is also worthwhile noting that an MRD without control performs worse than a linear viscous damper. This is due to the large forces at low velocity as well as to the large hysteresis in its characteristics.

Finally Figure 7.37 shows the transmissibility trends (RMS acceleration versus frequency) for upper and lower mass accelerations, superimposed on the response of the passive system. A reduction in the magnitude of the resonance peak is noticeable, which will produce an increase in comfort. The peak shift to about 1 Hz is beneficial as the body is a little less sensitive to vertical vibration at 1 Hz than at 1.5 Hz.

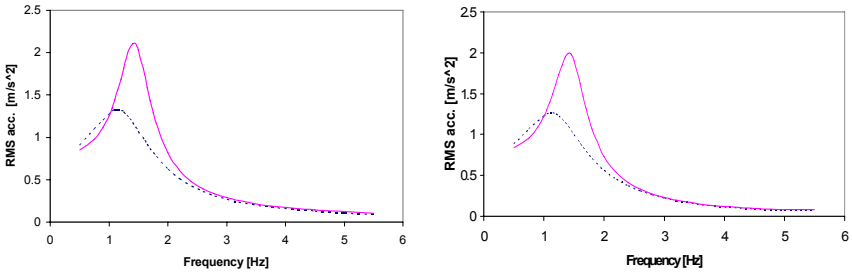

a b

Fig. 7.37. (a) Upper mass acceleration transmissibility; passive (———), fuzzy (- - - - -); (b) lower mass acceleration transmissibility; passive (———), fuzzy (- - - - -), [copyright Inderscience (2005), reproduced from Guglielmino E, Stammers CW, Stancioiu D, Sireteanu T and Ghigliazza R, Hybrid variable structure-fuzzy control of a magnetorheological damper for a seat suspension, International Journal of Vehicle Autonomous Systems, Vol. 3, N 1, used by permission]

7.5.2 Conclusions

The semi-active seat suspension with a controllable MRD can satisfactorily reduce the vertical acceleration experienced by the driver. By using the hybrid variable structure fuzzy control strategy a RMS reduction of about 21% is achieved. Using crisp control slightly better results can be obtained in terms of RMS but the spikes induced by the variable structure controller switching action worsen ride quality. In order to eliminate these spikes filtering would be necessary, but this would reduce the MRD bandwidth; fuzzy logic instead allows full use of the MRD bandwidth.

7.6 Case Study 3: Road Damage Reduction with MRD Truck Suspension

7.6.1 Introduction

Heavy vehicles travel over a variety of road surfaces and experience a wide range of vibration. This affects not only ride quality, but also causes road damage.

Weather conditions as well as vehicle motion are two key causes of road pavement damage. Road damage requires significant investment every year to repair the road surface and causes delays to traffic while it is being done.

Heavy vehicle suspensions ought to be able to isolate the sprung mass from road-induced disturbances as well as improving handling and minimising road damage by reducing dynamic tyre force within the constraint of a set working space.

The reduction of dynamic tyre forces is a challenging field. Cole and Cebon (1996a and 1996b) did extensive work on it, both theoretical and experimental. A thorough analysis of the damage due to dynamic tyre forces and other co-factors is presented by Cebon (1999): an instrumented vehicle was employed to measure the dynamic tyre forces at both low and high excitation frequencies. The study concluded that the wheel dynamic load increases with both vehicle speed and road roughness.

Algorithms are aimed at the reduction of tyre load oscillations, which improves handling on one hand and on the other reduces road damage caused by vehicle wheels. This latter application is particularly important in the case of heavy freight vehicles. Extended groundhook control logic was investigated by Valasek *et al.* (1998) to reduce dynamic tyre forces.

This case study presents a hybrid balance algorithm to reduce road damage and investigate the performance of a heavy articulated vehicle equipped with both MR dampers and passive viscous dampers. A half truck model is employed and system performance investigated via numerical simulation. A variation of the balance logic strategy based on dynamic tyre force tracking has been devised. Algorithm robustness to parametric variations as well as to real-life implementation issues such as feedback signals noise are discussed.

Given the modest cost of MR dampers compared to the overall cost of the vehicle, and the fact that road maintenance requires significant investment worldwide (an estimated of several hundred millions pounds of road damage in the UK was judged to be due to heavy vehicles; Potter *et al.*, 1995) these benefits are cost effective.

A model is developed for the semi-active control of the suspension of a three-axle tractor–trailer combination. Control is applied via an MR damper at either the tractor rear axle or the trailer axle. The load on the tractor front axle is smaller than that on the other two axles and is much less significant from the point of view of road damage.

Control reduces dynamic tyre forces and hence road damage, while improving handling. Trailer sprung mass acceleration (heave and pitch) is also reduced. Robustness of control is established by adding noise to the computed sensor inputs.

7.6.2 Half Truck and MR Damper Model

The half truck model is based on that described in Chapter 2 (Equations 2.31 and 2.32) and pictured in Figure 2.18. Lateral and yaw motions are neglected at this stage, reducing the model complexity. The roll motion is also neglected. Half truck vehicle parameters employed in the simulation are listed in Table 7.4.

The vehicle travels in a straight course with constant speed and is modelled as a three-axle vehicle, the steer axle, the drive tractor axle and the trailer axle, assuming two MR dampers, one fitted on the tractor drive axle and one on the trailer axle of the half truck; the steer axle is equipped with a passive viscous damper.

The objective is to investigate the vehicle performance in terms of ride and road damage using two semi-active dampers controlled by a hybrid logic for various road profiles. The MR damper model employed is based on the work by Lau and Liao (2005), who designed and modelled a prototype damper for a train suspension. Such a damper develops forces of the same order of magnitude as those required in a truck application and in this respect it could be potentially suitable for heavy vehicle applications as well. The schematic diagram of the damper model is shown in Figure 7.38.

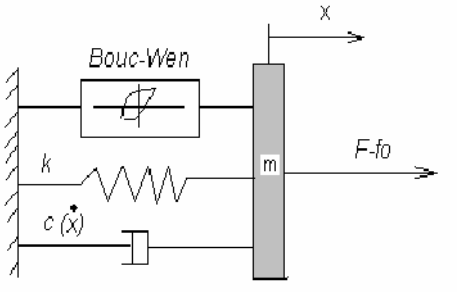

Fig.7.38. MR damper schematic model [copyright IMechE (2008), reproduced from Tsampardoukas G, Stammers CW and Guglielmino E, Semi-active control of a passenger vehicle for improved ride and handling, accepted for publication in Proceedings of the Institution of Mechanical Engineers, Part D: Journal of Automobile Engineering, Publisher: Professional Engineering Publishing, ISSN 0954/4070, Vol. 222, D3/2008, pp 325–352, used by permission]

It is a Bouc–Wen model coupled with a non-linear viscous damper with exponential characteristics and a linear spring term. The governing equations are as follows:

$$\dot{z} = -\gamma |\dot{x}| |z|^{n-1} z - \beta \dot{x} |z|^{n} + A \dot{x} , \tag{7.6}$$

$$C(\dot{x}) = -a_1 \exp(-a_2 |\dot{x}|)^{p} , \tag{7.7}$$

$$F - f_0 = az + kx + C(\dot{x})\dot{x} + m\ddot{x} . \tag{7.8}$$

Table 7.4. Key parameters employed in simulation (copyright Elsevier, reproduced from Tsampardoukas G, Stammers CW and Guglielmino E, Hybrid balance control of a magnetorheological truck suspension, accepted for publication in Journal of Sound and Vibration, used by permission)

Parameter	Value
Tractor chassis mass	$m_c = 4400$ kg
Trailer chassis mass (laden)	$m_t = 12500$ kg
Tractor pitch inertia	$J_c = 18311$ kgm^2
Trailer pitch inertia	$J_t = 251900$ kgm^2
Steer tractor unsprung mass	$m_{u1} = 270$ kg
Drive tractor unsprung mass	$m_{u2} = 520$ kg
Trailer unsprung mass	$m_{u3} = 340$ kg
Distance from steer tractor axle to tractor C.G.	$l_1 = 1.2$ m
Distance from tractor C.G. to drive tractor axle	$l_2 = 4.8$ m
Distance from tractor C.G. to articulation point	$l_4 = 4.134$ m
Distance from articulation point to trailer C.G.	$l_5 = 6.973$ m
Distance from trailer C.G. to trailer axle	$l_6 = 4$ m
Tyre stiffness of steer tractor wheel	$k_{tf} = 847$ kN/m
Tyre stiffness of drive tractor wheel	$k_{tr} = 2$ MN/m
Tyre stiffness of trailer wheel	$k_{tt} = 2$ MN/m
Suspension spring stiffness of steer tractor axle	$k_f = 300$ kN/m
Suspension spring stiffness of drive tractor axle	$k_r = 967430$ N/m
Suspension spring stiffness of trailer axle	$k_t = 155800$ N/m
Suspension damping rate of steer tractor axle	$c_f = 10$ kNs/m
Suspension damping rate of drive tractor axle	$c_r = 27627$ Ns/m
Suspension damping rate of trailer axle	$c_t = 44506$ Ns/m
Stiffness of articulated connection	$k_5 = 20$ MN/m
Damping of articulated connection	$c_5 = 200$ kNs/m

As explained in Chapter 2, the variable z is an evolutionary variable while the parameters β, γ, A and n define the shape of the hysteresis loop. Equation 7.7 models the post-yield plastic damping coefficient, which depends on the relative velocity. This equation is used to describe the MR fluid shear thinning effect, which results in the roll-off of the resisting force of the damper in the low-velocity region. The total exerted force is described by Equation 7.8, which takes into account the evolutionary variable z and the post-yield plastic model, expressed by

(7.7). Table 7.5 lists the numerical value of the constant parameters of the MRD (while the parameters a , a_1 , a_2 , n and f_o are current dependent).

Table 7.5. Constant parameters for MR damper (copyright Elsevier, reproduced from Tsampardoukas G, Stammers CW and Guglielmino E, Hybrid balance control of a magnetorheological truck suspension, accepted for publication in Journal of Sound and Vibration, used by permission)

Parameter	Value	Parameter	Value
γ	32000 m^{-2}	m	100 kg
β	22 m^{-2}	k	2500 N/m
A	220	p	0.54

The simulated characteristics are depicted in Figure 7.39.

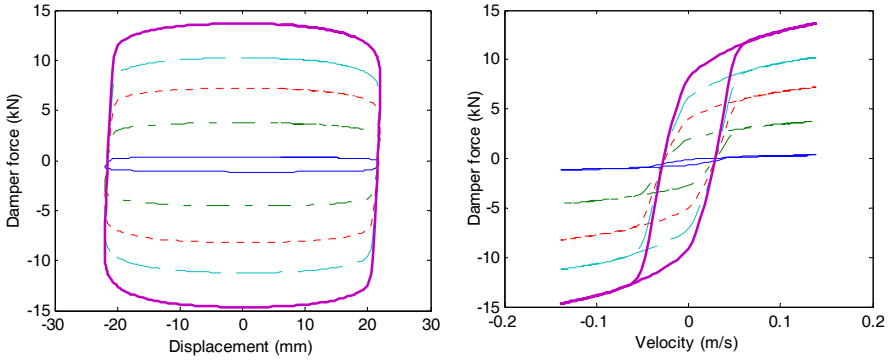

a b

Fig. 7.39. (a) MR damper force velocity and (b) force displacement characteristics for a 22-mm 1-Hz sinusoidal displacement excitation (copyright Elsevier, reproduced from Tsampardoukas G, Stammers CW and Guglielmino E, Hybrid balance control of a magnetorheological truck suspension, accepted for publication in Journal of Sound and Vibration, used by permission)

A benchmark viscous damper having different damping coefficients for the bound and rebound strokes was used (the equivalent damping ratios are, respectively, 0.15 and 0.35).

Appropriate road profile models are required to assess truck performance under realistic operative conditions. Two types of road are considered in this case study: a smooth highway and a highway with gravel. The spectral densities of both road profiles are expressed by $S_g(\Omega)=C_{sp}\Omega^{-n}$, the parameters C_{sp} and n determining the road quality. The smooth highway is described by n = 2.1 and $C_{sp}=4.8\cdot\times 10^{-7}$ whereas the gravel road is determined by setting $C_{sp}=4.4\cdot\times 10^{-6}$ and n = 2.1 (Wong, 1993). Heavy goods vehicles are mainly designed to operate on smooth rather than on poor roads. The vehicle operation on highway with gravel is a scenario to

examine the performance of the semi-active suspension on damaged roads or in off-road operation.

7.6.3 Road Damage Assessment

It is of paramount importance to establish a quantitative criterion to assess road damage (Cebon, 1989). The most widely employed is the *fourth power law*. This is a result of the experimental work undertaken by the American Association of State Highway and Transportation Officials (AASHO) (Gillespie, 1985). This law shows that the pavement serviceability decreases every time a heavy vehicle axle passes on the road. This reduction is assumed to be related to the fourth power of its static load (Cebon, 1999). Another criterion is known as the *aggregate fourth power force* (Cole *et al.*, 1994) while Potter *et al.* (1995) give a simplified approach to road damage. It is expressed by the following formula:

$$A_k^n = \sum_{j=1}^{Na} P_{jk}^n \ , \tag{7.9}$$

where k =1, 2, 3,…, Na is the location along the road. The exponent n is chosen depending upon the type of pavement and ranges from n = 4 (suitable for fatigue damage) to n = 1 (permanent deformation caused by static load). In this work in order to describe the fatigue damage, the aggregate fourth power law with n = 4 is used, normalised with respect to the static force *i.e.*,

$$A_k^4 = \sum_{j=1}^{Na} \left(\frac{\text{Static force + Dynamic force}}{\text{Static force}} \right)_{jk}^4 \tag{7.10}$$

7.6.4 Road Damage Reduction Algorithm

The algorithm outlined here is a variant of the balance logic described in Chapter 4. This hybrid version aims at cancelling the drive tractor and trailer axle tyre forces. The essence of the proposed control algorithm is to cancel the tyre force fluctuations on each axle by ensuring that the wheel follows the road profile closely. The dynamic tyre forces are balanced by applying a controlled damping force in the opposite direction. This is only possible when the control force and the relative velocity have opposite signs and hence energy dissipation takes place.

$$Fc_{\text{rear}} = \begin{cases} b_{\text{r}}\left(-F_{\text{sr}} - m_{u2}\ddot{x}_{\text{wr}}\right) + b_2 F_{\text{dr}} & \text{if} \quad Fc_{\text{rear}} \cdot \text{rear\_rel\_vel} < 0 \\ b_3 F_{\text{dr}} & \text{if} \quad Fcr_{\text{rear}} \cdot \text{rear\_rel\_vel} > 0 \end{cases} \tag{7.11}$$

$$Fc_{\text{trailer}} = \begin{cases} b_{\text{t}}\left(-F_{\text{st}} - m_{u3}\ddot{x}_{\text{wt}}\right) + b_2 F_{\text{dt}} & \text{if} \quad Fc_{\text{trailer}} \cdot \text{trailer\_rel\_vel} < 0 \\ b_3 F_{\text{sd}} & \text{if} \quad Fc_{\text{trailer}} \cdot \text{trailer\_rel\_vel} > 0 \end{cases} \tag{7.12}$$

A pseudo-viscous damping term is added to the control forces to reduce transients, particularly when inputs are near to the wheel-hop frequency. Studies (not reported here) have indicated that the optimal values of b_2 and b_3 (to minimise road damage) should be 20% of critical passive damping when the vehicle travels on smooth or gravel roads. Smaller or higher values of b_2 and b_3 result in larger dynamic tyre forces and higher vibration levels. However, the optimum values of those parameters (in terms of road damage) alter when the vehicle wheels come into contact with bumps or potholes.

7.6.5 Time Response

In this section, and in the following ones, the response of the semi-active controlled MRD system is benchmarked against the passive system. The performance of the controlled system is assessed numerically both in the time domain and in the frequency domain.

The time response to a sinusoidal road surface is firstly investigated. Figures 7.40–7.42 depict the time histories for a 5-mm 2-Hz sinusoidal road input. The hybrid control logic significantly reduces the dynamic tyre forces of the tractor drive and trailer axles. The same trend is also observed for the trailer chassis acceleration. In contrast, the controlled suspension increases the chassis acceleration of the tractor unit. As expected a higher harmonic content is present in the semi-active time trends.

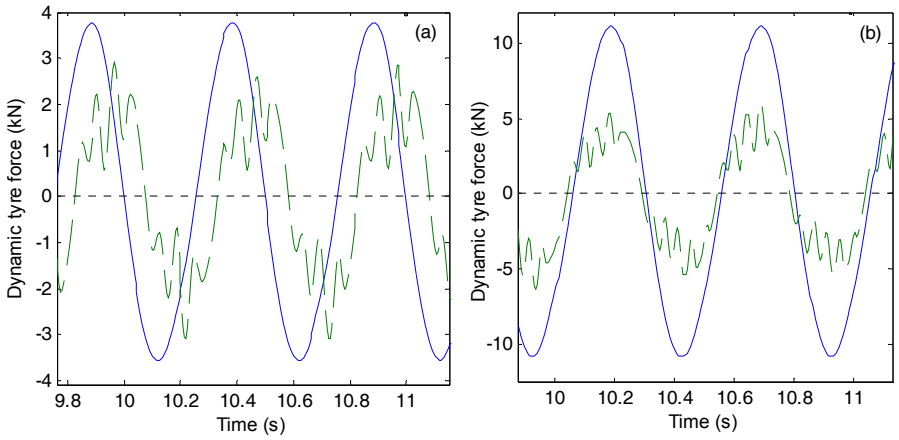

a b

Fig. 7.40. Dynamic tyre forces on tractor drive and trailer axles: (a) dynamic tyre force of tractor drive axle; (b) dynamic tyre forces of trailer axle; (- - - - -) semi-active suspension, (——) passive suspension (copyright Elsevier, reproduced from Tsampardoukas G, Stammers CW and Guglielmino E, Hybrid balance control of a magnetorheological truck suspension, accepted for publication in Journal of Sound and Vibration, used by permission)

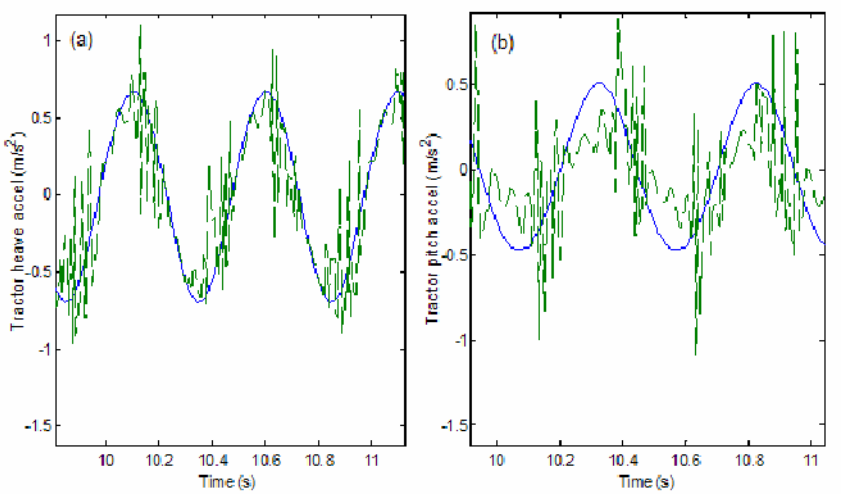

a b

Fig. 7.41. Tractor and trailer chassis heave acceleration: (a) tractor chassis heave acceleration; (b) tractor chassis pitch acceleration; (- - - - -) semi-active suspension, (——) passive suspension (copyright Elsevier, reproduced from Tsampardoukas G, Stammers CW and Guglielmino E, Hybrid balance control of a magnetorheological truck suspension, accepted for publication in Journal of Sound and Vibration, used by permission)

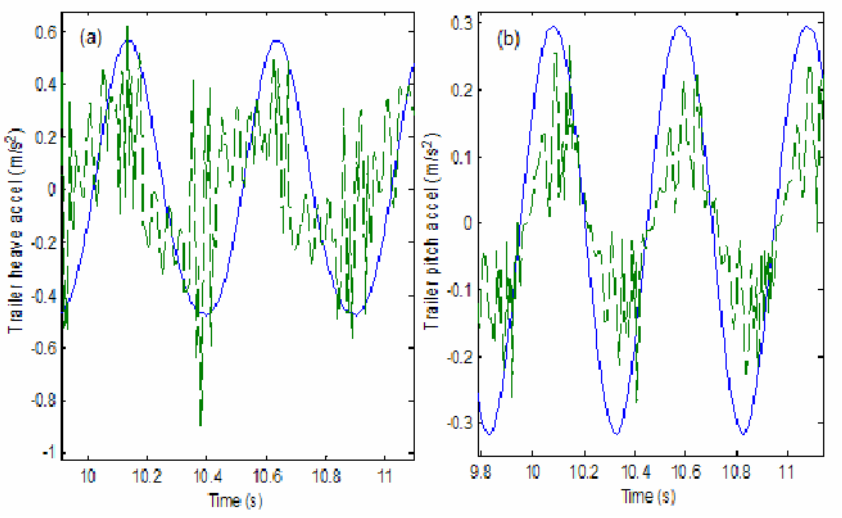

a b

Fig. 7.42. Trailer chassis heave and pitch accelerations (a) trailer chassis heave acceleration; (b) trailer chassis pitch acceleration; (- - - - -) semi-active suspension, (——) passive suspension (copyright Elsevier, reproduced from Tsampardoukas G, Stammers CW and Guglielmino E, Hybrid balance control of a magnetorheological truck suspension, accepted for publication in Journal of Sound and Vibration, used by permission)

7.6.6 Truck Response on Different Road Profiles

The percentage reduction achieved by the semi-active case relative to both passive cases (MRD with current I = 0 A and passive viscous damping) is given by Figures 7.43 and 7.44 for vehicle accelerations and road damage. The benefits of semi-active control are evident, particularly at moderate speed, but limited in regard to road damage because the predominant load (and hence damage) is the static one.

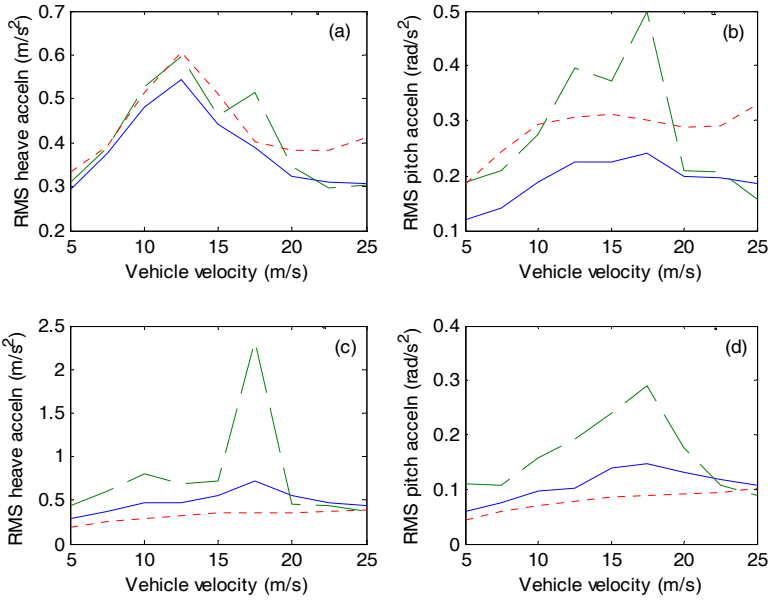

Fig. 7.43. RMS heave and pitch accelerations: (a) tractor chassis; (b) tractor chassis; (c) trailer chassis; (d) trailer chassis; (——) conventional passive viscous damper, (— —) passive MR damper (current = 0 A), (- - - -) semi-active MR damper (copyright Elsevier, reproduced from Tsampardoukas G, Stammers CW and Guglielmino E, Hybrid balance control of a magnetorheological truck suspension, accepted for publication in Journal of Sound and Vibration, used by permission)

The semi-active MR damper significantly reduces the trailer unit heave and pitch accelerations. This is due to the improved isolation achieved by the two MR dampers fitted on the drive tractor and trailer axles. However, at high vehicle speed the semi-active suspension degrades the vehicle performance in terms of tractor chassis accelerations. This occurs because the controllable damper is installed only on the drive tractor axle. It has been verified that the tractor performance would improve if a third MR damper was fitted on the steer axle as well. However truck driver seat are often equipped with a seat damper (ideally semi-active; see case study 2), which in practice reduces the vibration level experienced by the driver.

The application of the road damage criterion given in Figure 7.44 reveals that the damage caused by the dynamic tyre forces is significantly reduced when the balance control cancels them by 100%, while the coefficients b_2 and b_3 are equal to 0.2 of the critical damping force. Figure 7.44 shows that the semi-active suspension reduces significantly the road damage caused by each individual axle as well as the total vehicle damage. It is important to note that the vehicle suspension employing passive MR dampers (*i.e.*, $I = 0$ A) degrades the vehicle response due to its low damping.

The amount of dynamic tyre force cancellation is a critical parameter which affects the system response as Figure 7.45 shows. At low and medium vehicle velocities 100% cancellation is the best option because both RMS and max dynamic tyre forces at each axle are significantly reduced relative to the passive system, resulting in lower road damage with respect to the damage criterion used. On the other hand, it is beneficial to reduce the amount of cancellation for the damper fitted on the drive tractor axle in order to improve tractor unit comfort, particularly at high vehicle velocities, but such a reduction adversely affects road damage at high velocities. Consequently, the optimal choice for the amount of spring force cancellation depends on the control objective.

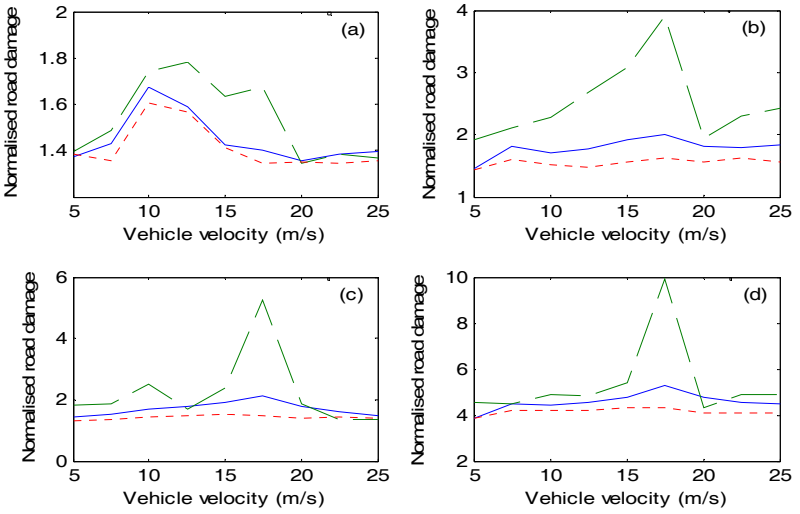

Fig. 7.44. Maximum normalised road damage: (a) steer axle; (b) drive axle; (c) trailer axle; (d) total vehicle: (———) passive viscous damper, (— —) passive MR damper (current = 0 A), (- - - -) semi-active MR damper (copyright Elsevier, reproduced from Tsampardoukas G, Stammers CW and Guglielmino E, Hybrid balance control of a magnetorheological truck suspension, accepted for publication in Journal of Sound and Vibration, used by permission)

A design solution which achieves a compromise between these two requirements entails the use of a suspended driver cab and seat to help reduce the vibration

levels transmitted to the human body. In that case, 100% cancellation is the best solution in terms of lower maximum dynamic tyre forces for the semi-active device located at the tractor drive axle, while 50% cancellation is the best solution overall for the same device at the trailer axle. The variation between the amount of cancellation between the units is mainly affected by the coupled vehicle motion and the model (half truck) used. Consequently, a full truck model should be developed in order to evaluate the performance of the hybrid control logic not only for ride but also for handling manoeuvres.

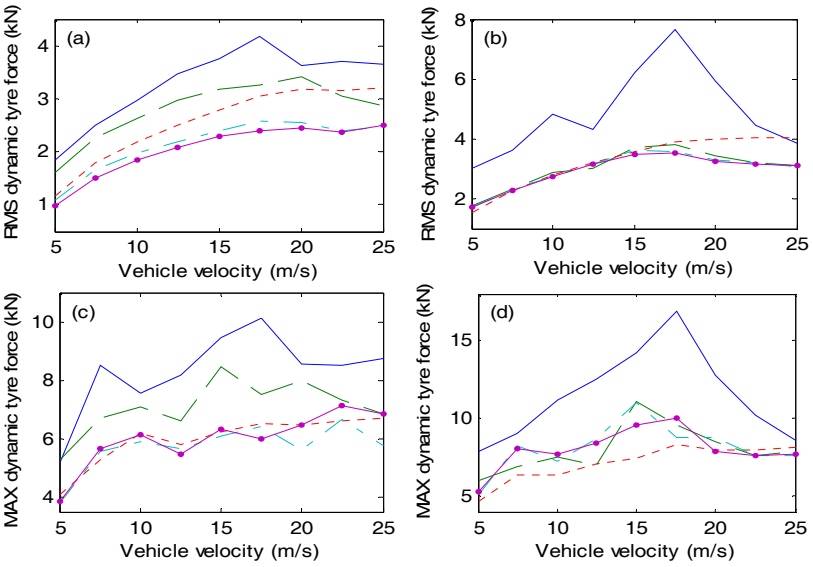

Fig. 7.45. RMS and max dynamic tyre forces due to partial cancellation: (a) tractor drive axle; (b) trailer axle; (c) tractor drive axle; (d) trailer axle. (———) passive viscous damper, (— —) semi-active 25% cancellation, (- - - -) semi-active 50% cancellation, (— - —-) semi-active 75% cancellation, (———●———) semi-active 100% cancellation (copyright Elsevier, reproduced from Tsampardoukas G, Stammers CW and Guglielmino E, Hybrid balance control of a magnetorheological truck suspension, accepted for publication in Journal of Sound and Vibration, used by permission)

The vehicle performance is now investigated when the vehicle operates on a gravel road. A smooth road surface may have sections where the surface is rough due to maintenance or resurfacing work. It is essential to assess the vehicle and the control logic behaviour under these conditions. Heavy good vehicles are mainly designed to operate on smooth highways rather than on poor roads. Consequently, the vehicle operation on highway with gravel is a scenario to assess the performance of the semi-active suspension either off-road or under large amplitude-road inputs.

Simulation results show that the heave and pitch accelerations of the tractor and trailer units are reduced by control. Figure 7.46 presents the dynamic tyre forces of the vehicle in three different cases. The semi-active suspension performs better

than the passive system over the velocity range investigated; however, the control logic becomes ineffective when the vehicle velocity is higher than 25 m/s. The vehicle performance is similar to that on smooth road in terms of normalised road damage.

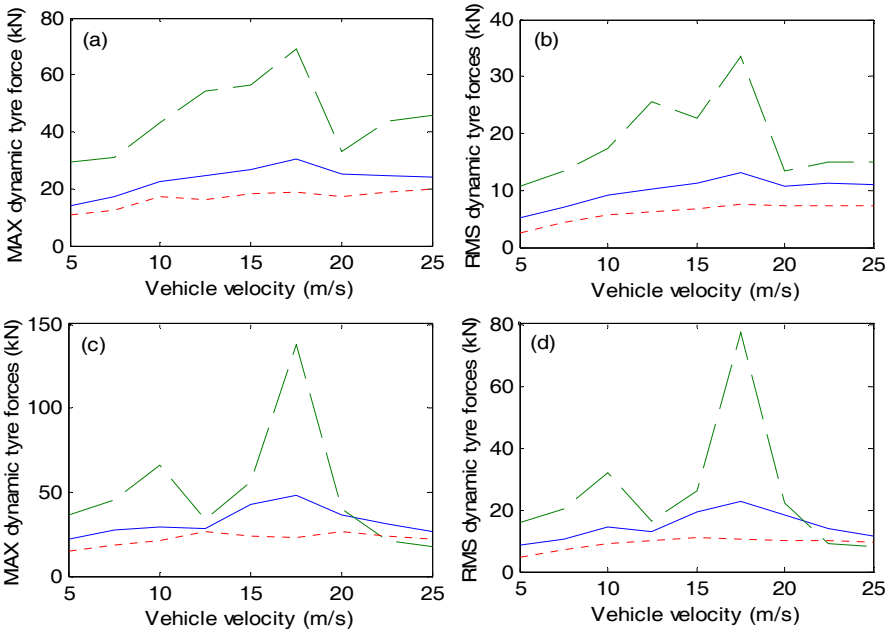

Fig. 7.46. Dynamic tyre forces: (a) tractor drive axle; (b) tractor drive axle; (c) trailer axle; (d) trailer axle; (——) passive viscous damper, (— —) passive MR damper (I = 0 A), (- - - -) semi-active MR damper (copyright Elsevier, reproduced from Tsampardoukas G, Stammers CW and Guglielmino E, Hybrid balance control of a magnetorheological truck suspension, accepted for publication in Journal of Sound and Vibration, used by permission)

The results presented so far can be summarised as follows:

- Semi-active hybrid balance control is beneficial to heavy vehicle performance: chassis accelerations are significantly reduced and road damage moderately so,
- The semi-active MR damper significantly reduces axle loads at all speeds on both harsh and smooth roads,
- By employing balance logic on the drive tractor and trailer controlled dampers, trailer chassis acceleration is substantially reduced. The tractor chassis acceleration slightly increases because a passive viscous damper is used on the steer tractor axle,
- The partial cancellation of the dynamic tyre forces is mainly affected by the vehicle speed; 100% cancellation is the optimal solution in terms of lower road damage in the moderate vehicle speed range (from 12.5 m/s to 20 m/s) while 75% cancellation is the best solution in the low (from 5m/s to 10m/s) and high vehicle speed ranges (from 20 m/s to 25 m/s),

- The passive MR damper is not able to produce high forces, causing excessive load on axles. However an MR damper operates in this mode only because of an electrical fault (*e.g.*, if the control system power supply fails). The system performs poorly but this is a provisional fail-safe condition. The on-board electronics will spot the failure immediately, warning the driver.

7.6.7 Truck Response to Bump and Pothole

The vehicle response to bump and to pothole inputs is another essential test to assess suspension performance. The bump and pothole are modelled as follows (Pesterev *et al.*, 2002):

$$r(s) = \begin{cases} -\frac{a}{2}(1 - \cos\frac{2\pi s}{b}) & 0 \le s \le b \\ 0 & s < 0,\ s > b \end{cases} \tag{7.13}$$

The parameters a and b determine the depth and the width of the pothole, while the negative value of a corresponds to a bump. Table 7.6 lists the parameters used in the results presented subsequently.

Table 7.6. Parameters for bump and pothole

Pothole	**Bump**
$a = 0.008$ m	$a = -0.008$ m
$b = 1$ m	$b = 1$ m
Vehicle velocity = 10 m/s	
100% cancellation of dynamic tyre forces $b_r = 1$ and $b_t = 1$	
$b_2 = 0.5$, amount of additional critical damper force when damper is on $b_3 = 0.2$, amount of critical damper force when damper is off	

Figures 7.47 and 7.48 show that the semi-active control scheme reduces the peak values of the dynamic tyre forces on both drive tractor and trailer axles. The controlled suspension reduces the number of oscillations with respect to the passive suspension. Similar trends can be observed for vehicle speeds ranging from 5 to 25 m/s (results not shown here). Control produces high damping during the settling time but more or less the same level of damping as the passive case during the impact stage.

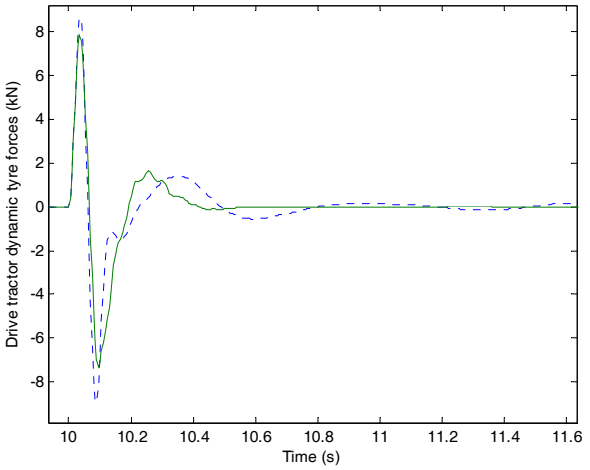

Fig. 7.47. Tractor drive dynamic tyre forces due to bump; (- - - - -) passive suspension, (——) semi-active suspension (copyright Elsevier, reproduced from Tsampardoukas G, Stammers CW and Guglielmino E, Hybrid balance control of a magnetorheological truck suspension, accepted for publication in Journal of Sound and Vibration, used by permission)

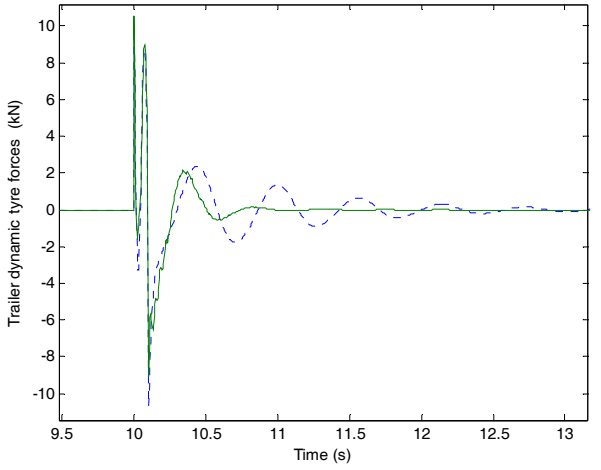

Fig. 7.48. Trailer drive dynamic tyre forces due to bump; (- - - - -) passive suspension, (——) semi-active suspension (copyright Elsevier, reproduced from Tsampardoukas G, Stammers CW and Guglielmino E, Hybrid balance control of a magnetorheological truck suspension, accepted for publication in Journal of Sound and Vibration, used by permission)

Simulation has also shown that an improvement is present on the trailer body heave and pitch accelerations too (graphs not depicted here): the free oscillations

are significantly reduced with the semi-active control as this results in an additional damping. However, the controlled tractor body heave and the pitch accelerations (graphs not shown here) are not any better than those with the passive suspension. In fact, the semi-active suspension increases the peak values of the heave and pitch accelerations. This is not unexpected because the control logic also increases the tractor body pitch acceleration. Analogous reults have been obtained in response to a pothole input.

7.6.8 Robustness Analysis

Instrumentation noise (due to electromagnetic interference, electrical component damage or any other reason) is a real-life issue. The algorithm robustness to injected white noise into the control loop is examined. White noise is added to feedback signals, *i.e.*, measured relative velocity and the axle heave acceleration. The level of noise is indicated on the velocity signal in Figure 7.49 for a vehicle velocity of 15 m/s.

A measure of how noise can degrade the overall performance is the increase in the number of switches of the controller (*i.e.*, increased chattering)

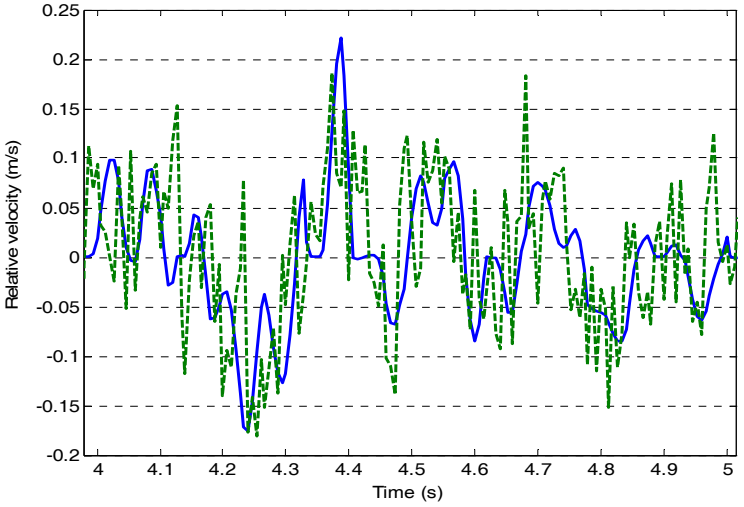

Fig. 7.49. Relative velocity across the tractor drive semi-active damper; (——) signal without added noise, (— —) signal with noise (copyright Elsevier, reproduced from Tsampardoukas G, Stammers CW and Guglielmino E, Hybrid balance control of a magnetorheological truck suspension, accepted for publication in Journal of Sound and Vibration, used by permission)

A moderate penalty due to noise is observed in the heave tractor chassis acceleration.

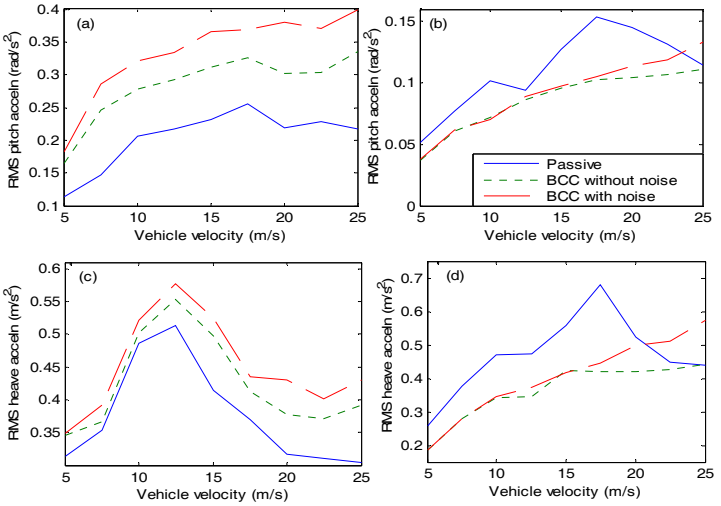

Fig. 7.50. Chassis RMS heave and pitch acceleration on both vehicle units: (a) tractor chassis; (b) trailer chassis; (c) tractor chassis; (d) trailer chassis; (———) passive, (- - - -) semi-active (BCC) without imposed noise, (— —) semi-active (BCC) with noise (copyright Elsevier, reproduced from Tsampardoukas G, Stammers CW and Guglielmino E, Hybrid balance control of a magnetorheological truck suspension, accepted for publication in Journal of Sound and Vibration, used by permission)

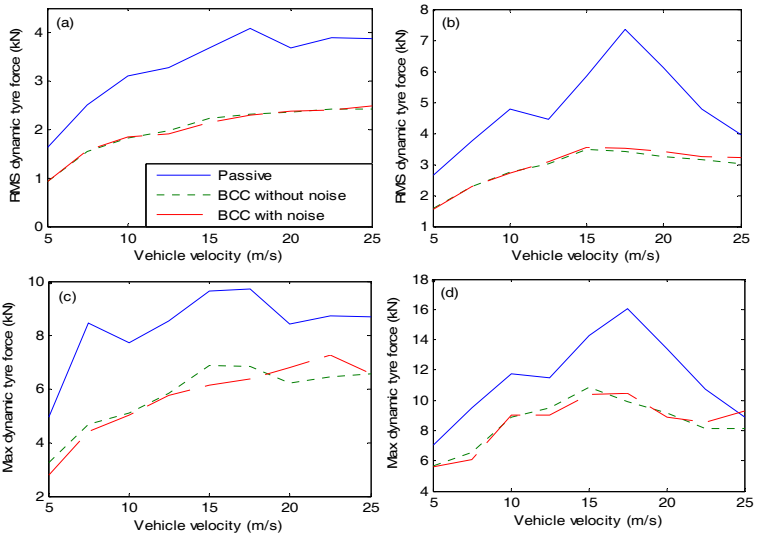

Fig. 7.51. RMS and max dynamic tyre forces on tractor drive and trailer axles: (a) tractor drive axle; (b) trailer axle; (c) tractor drive axle; (d) trailer axle; (———) passive, (- - - -) semi-active (BCC) without imposed noise, (— —) semi-active (BCC) with noise (copyright Elsevier, reproduced from Tsampardoukas G, Stammers CW and Guglielmino E, Hybrid balance control of a magnetorheological truck suspension, accepted for publication in Journal of Sound and Vibration, used by pemission)

The system response in respect of chassis acceleration, depicted in Figure 7.50, is somehow affected by the presence of noise: the heave and pitch acceleration of the trailer drive in the semi-active case are slightly increased relative to the semi-active case without noise.

Finally the RMS and maximum dynamic tyre forces on each axle are examined from the algorithm robustness angle. Figure 7.51 shows that the imposed noise only moderately affects the peak tyre forces, and has almost no effect on the RMS values. Consequently, the system performance in terms of dynamic tyre forces, comparing both semi-active cases, is not significantly influenced by the imposed noise to the feedback signals.

A reduction in the number of switches is essential to avoid over-heating and wear, and reduce component life. The switches between the on and off state in the two cases are measured and compared. For graphic clarity only, the on state of the semi-active damper is equal to unity while the off state is designated zero. Simulation results show that the semi-active case with the added noise increase the chattering as observed in Figure 7.52 in the time interval 3.7–4.2 s.

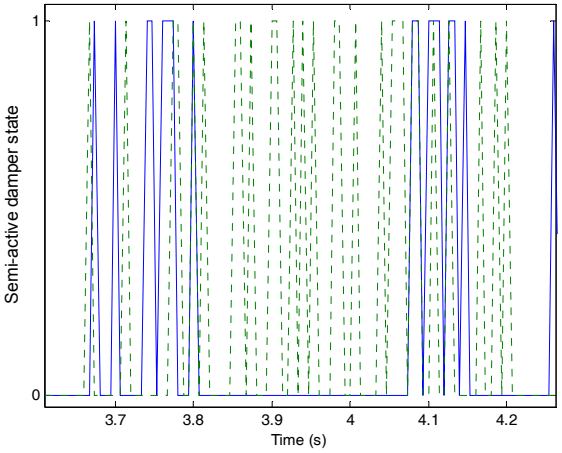

Fig. 7.52. On/off states of the semi-active damper; (——) semi-active (BCC without noise), (- - - -) semi-active (BCC with noise) (copyright Elsevier, reproduced from Tsampardoukas G, Stammers CW and Guglielmino E, Hybrid balance control of a magnetorheological truck suspension, accepted for publication in Journal of Sound and Vibration, used by permission)

7.6.8.1 Trailer Mass Variation

The payload in a truck can vary significantly (either fully loaded, partially loaded or unladen). The effects of the trailer mass variations are vital in terms of road damage. For the passive half vehicle model, the mass of the unladen trailer was taken as 5000 kg, the fully loaded trailer 12500 kg and a partly-loaded trailer 8500 kg.

The variations of the trailer mass are considered in the simulation process to examine the response of the system in the three cases. Figure 7.53 shows the reduction of the dynamic forces at a specified vehicle speed when the three

different trailer masses A convergence in the trends is observed at high vehicle speeds.

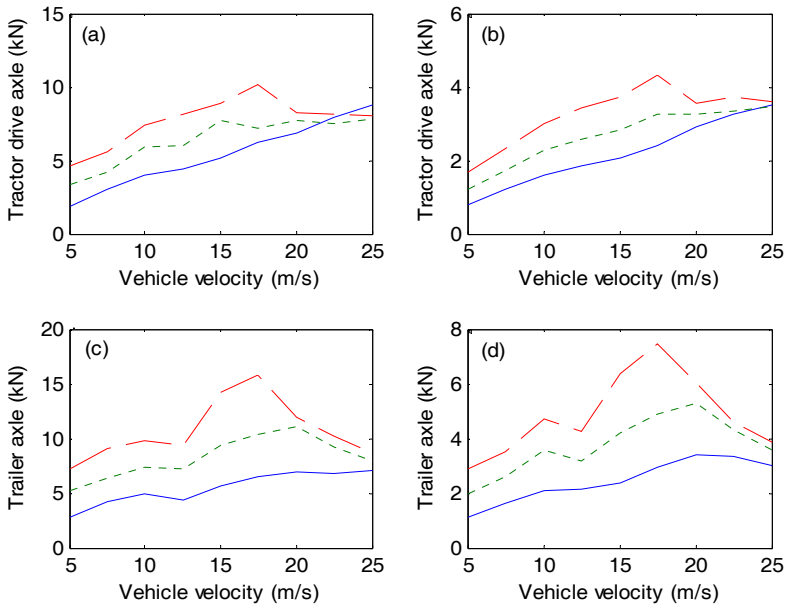

Fig. 7.53. Dynamic tyre forces for different values of the trailer mass: (a) maximum values; (b) RMS values; (c) maximum values; (d) RMS values; (——) m_t = 5000 kg, (- - - -) m_t = 8500 kg, (— —) m_t = 12500 kg (copyright Elsevier, reproduced from Tsampardoukas G, Stammers CW and Guglielmino E, Hybrid balance control of a magnetorheological truck suspension, accepted for publication in Journal of Sound and Vibration, used by permission)

7.6.8.2 Tyre Stiffness Variation

In order to simulate the vertical tyre motion due to road irregularities the tyre is modelled as a spring with high stiffness. In real operating conditions the tyre pressure is not constant and slowly changes over time, resulting in variations of the tyre stiffness. A tyre stiffness of 2 MN/m has normally been used in the simulation, while lower or higher values result in different tyre pressures.

The variation of the tyre stiffness of the drive tractor wheel shows that the dynamic tyre forces are slightly affected at low and moderate vehicle speeds (Figure 7.54). The system response alters at high vehicle velocities, producing larger tyre forces, resulting in higher road damage (as expressed by Equation 7.9). The simulation results plotted in Figure 7.54 show that the dynamic tyre forces at both axles are little affected by this variation. Consequently, the road damage (see road damage criterion) is also unaffected at low vehicle speeds with a moderate increase at high vehicle velocities.

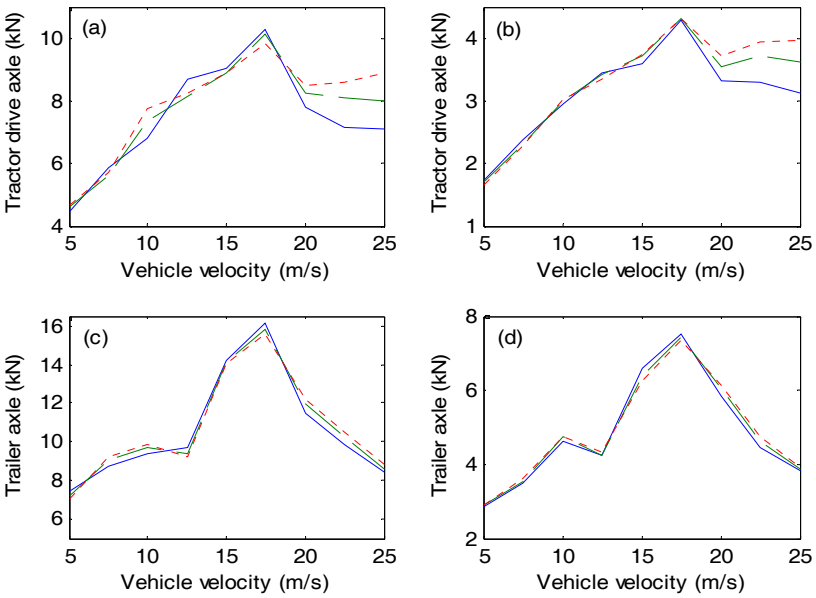

Fig. 7.54. Dynamic tyre forces for different values of the tyre stiffness: (a) maximum values; (b) RMS values; (c) maximum values: (d) RMS values; (——) k_{tr} = 1.6 MN/m, (— —) k_{tr} = 2 MN/m, (- - - -) k_{tr} = 2.4 MN/m (copyright Elsevier, reproduced from Tsampardoukas G, Stammers CW and Guglielmino E, Hybrid balance control of a magnetorheological truck suspension, accepted for publication in Journal of Sound and Vibration, used by permission)

7.6.8.3 MRD Response Time

The response time of MR dampers for vehicle applications is a critical factor because it determines the effectiveness of the MR damper used. The aim is now to assess the effect of the damper response to the vehicle performance.

The response time is defined as the time required for the MR damper to reach 64% or 95% (Goncalves *et al.*, 2003) of the final exerted force, starting from the initial state. The time response depends both on the fluid transformation from a mineral-oil-like consistency (but not majorly as this time is less than 1 ms) and on the inductance of the electromagnetic circuit as well as the output impedance of the driving electronics.

Extensive experimental work by Koo *et al.* (2004) showed that the time response of the MR damper is affected by several parameters such as the response of the driving electronics, the applied current, the piston velocity and the system compliance. The time response of MR damper for commercial vehicle application is less than 25 ms (effective time response to reach 95% of its final value).

In the simulation work a first-order lag is employed in the semi-active control schemes in order to model the MR damper dynamics. The time constant of the first-order lag is chosen so that the system reaches 64% of the final value in 11 ms (one time constant), which corresponds to 25 ms to reach 95% of its final value

(effective time constant). In the current study the time constant quoted is that to reach 64% of the final state.

Simulation results indicate that a fast-response MR damper (5 ms time constant) is the preferable device to improve the vehicle response in terms of lower dynamic tyre forces. Figure 7.55 shows that the maximum values rather than the RMS values of the dynamic tyre forces are more sensitive to the time response of the semi-active damper.

A damper with time constant equal to 20 ms produces larger maximum tyre forces because it cannot respond fast enough to exert the required control force in order to cancel the dynamic tyre forces.

However, the latter value of the time constant is high and is the typical of a bigger damper, more suitable for controlling structural vibration. A time constant of 15 ms, which corresponds to a 37.5 ms effective time constant, might be a more realistic value for semi-active dampers used in heavy-vehicle applications.

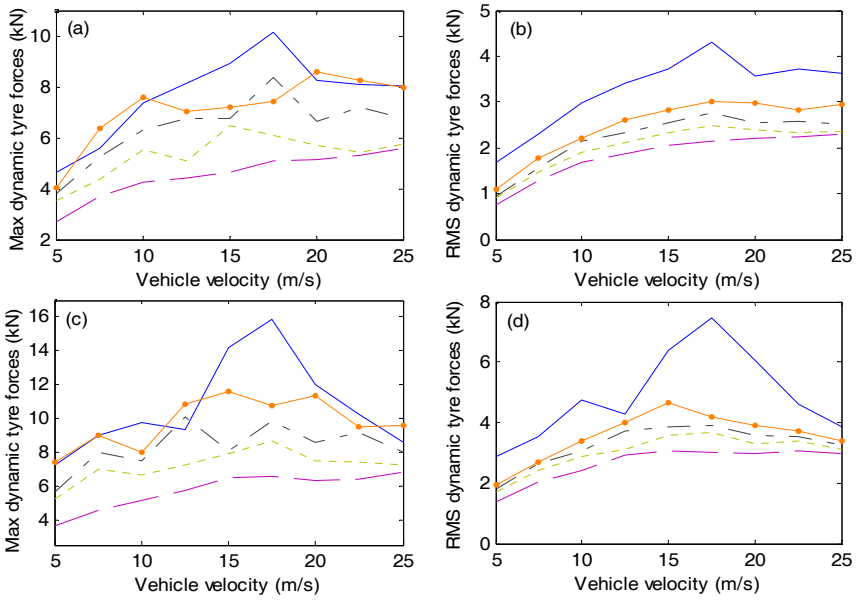

Fig. 7.55. Max dynamic tyre forces for different time constants: (a) tractor drive axle; (b) tractor drive axle; (c) trailer axle; (d) trailer axle; (——) passive damper, (— —) Tc = 5 ms (- - - -), Tc = 10 ms (— - — -), Tc = 15 ms (—●—), Tc = 20 ms (copyright Elsevier, reproduced from Tsampardoukas G, Stammers CW and Guglielmino E, Hybrid balance control of a magnetorheological truck suspension, accepted for publication in Journal of Sound and Vibration, used by permission)

7.7 Conclusions

This case study centred on road damage reduction has shown that the semi-active truck suspension response is superior overall to the passive response on both road profiles (smooth and gravel). The maximum and RMS values of the dynamic tyre forces are substantially reduced by the control logic and the road damage follows the same pattern as the dynamic tyre forces. Similarly, a reduction of the trailer chassis acceleration is obtained because the trailer unit is well isolated from the ground irregularities. Conversely, the tractor chassis acceleration slightly increases because the steer axle is assumed to be equipped with conventional viscous dampers.

Additionally, the simulation results show that the MRD has poor performance when the applied current is zero (passive operation) due to the very low damping provided by the semi-active device. However, this scenario occurs only in the event of a failure of the MRD control system hardware.

The partial cancellation of the dynamic tyre forces is also examined to establish the optimal amount of cancellation on smooth and gravel road profiles while the other control parameters (b_2 and b_3) are kept constant. The results indicate that 100% cancellation of tyre force fluctuation is always preferable in terms of lower road damage and dynamic tyre force fluctuations.

The vehicle was also tested with pothole and bump inputs. The results show that the semi-active suspension with the hybrid control algorithm reduces the amplitude of the free oscillations while the peak values of dynamic tyre forces are slightly reduced. Also, the vehicle response is mainly affected by the parameter b_2 rather than the amount of cancellation.

From a robustness viewpoint, chassis accelerations and the RMS dynamic tyre forces are slightly affected by imposed noise while the maximum values of the dynamic tyre forces are slightly affected at moderate vehicle velocities. Robustness to sprung and unsprung mass variation was also assessed and the algorithm was found to be not very sensitive to noise.

In terms of dynamic response a fast-response semi-active damper (one time constant equal to 5 ms) is extremely beneficial in reducing dynamic tyre forces. However, this value of time constant is optimistic not only for a large force damper needed for heavy vehicles but also for dampers suitable for passenger vehicles.